JGR Space Physics

RESEARCH ARTICLE
10.1029/2020JA028707

A Comparison of Radial Diffusion Coefficients in 1-D and 3-D Long-Term Radiation Belt Simulations

A. Y. Drozdov[1], H. J. Allison[2], Y. Y. Shprits[1,2,3], S. R. Elkington[4], and N. A. Aseev[2,3]

[1]University of California Los Angeles, Los Angeles, CA, USA, [2]GFZ German Centre for Geosciences, Potsdam, Germany, [3]Institute of Physics and Astronomy, University of Potsdam, Potsdam, Germany, [4]Laboratory for Atmospheric and Space Physics, University of Colorado Boulder, Boulder, CO, USA

Key Points:

- 3-D simulations using different radial diffusion coefficients, except Ali et al. (2016), produce similar results
- Using Ali et al. (2016) D_{LL}, simulated flux is significantly lower than observations
- 3-D modeling with Brautigam and Albert (2000) D_{LL} results in a slightly smaller normalized difference (averaged over energies) to observations

Supporting Information:

Supporting Information may be found in the online version of this article.

Correspondence to:

A. Drozdov and H. Allison,
adrozdov@ucla.edu;
haylis@gfz-potsdam.de

Citation:

Drozdov, A. Y., Allison, H. J., Shprits, Y. Y., Elkington, S. R., & Aseev, N. A. (2021). A comparison of radial diffusion coefficients in 1-D and 3-D long-term radiation belt simulations. *Journal of Geophysical Research: Space Physics*, *126*, e2020JA028707. https://doi.org/10.1029/2020JA028707

Received 29 SEP 2020
Accepted 12 JUL 2021

Abstract Radial diffusion is one of the dominant physical mechanisms driving acceleration and loss of radiation belt electrons. A number of parameterizations for radial diffusion coefficients have been developed, each differing in the data set used. Here, we investigate the performance of different parameterizations by Brautigam and Albert (2000), https://doi.org/10.1029/1999ja900344, Brautigam et al. (2005), https://doi.org/10.1029/2004ja010612, Ozeke et al. (2014), https://doi.org/10.1002/2013ja019204, Ali et al. (2015), https://doi.org/10.1002/2014ja020419; Ali et al. (2016), https://doi.org/10.1002/2016ja023002; Ali (2016), and Liu et al. (2016), https://doi.org/10.1002/2015gl067398 on long-term radiation belt modeling using the Versatile Electron Radiation Belt (VERB) code, and compare the results to Van Allen Probes observations. First, 1-D radial diffusion simulations are performed, isolating the contribution of solely radial diffusion. We then take into account effects of local acceleration and loss showing additional 3-D simulations, including diffusion across pitch-angle, energy, and mixed diffusion. For the L* range studied, the difference between simulations with Brautigam and Albert (2000), https://doi.org/10.1029/1999ja900344, Ozeke et al. (2014), https://doi.org/10.1002/2013ja019204, and Liu et al. (2016), https://doi.org/10.1002/2015gl067398 parameterizations is shown to be small, with Brautigam and Albert (2000), https://doi.org/10.1029/1999ja900344 offering the smallest averaged (across multiple energies) absolute normalized difference with observations. Using the Ali et al. (2016), https://doi.org/10.1002/2016ja023002 parameterization tended to result in a lower flux than both the observations and the VERB simulations using the other coefficients. We find that the 3-D simulations are less sensitive to the radial diffusion coefficient chosen than the 1-D simulations, suggesting that for 3-D radiation belt models, a similar result is likely to be achieved, regardless of whether Brautigam and Albert (2000), https://doi.org/10.1029/1999ja900344, Ozeke et al. (2014), https://doi.org/10.1002/2013ja019204, and Liu et al. (2016), https://doi.org/10.1002/2015gl067398 parameterizations are used.

1. Introduction

Fluctuations in the magnetic and electric fields result in diffusive motion of radiation belt electrons across Roederer's L* parameter (Fälthammar, 1965; Roederer, 1970), a version of the third adiabatic invariant. L* diffusion (henceforth referred to as radial diffusion) occurs at constant first and second adiabatic invariants, and the electron's energy is increased (reduced) with diffusion into regions of stronger (weaker) magnetic field. Much of the dynamics of the radiation belts can be attributed to radial diffusion and the subsequent energy change of the electron populations (Shprits et al., 2008), so understanding the rate of the diffusion is a vital factor for accurately predicting and reconstructing the evolution of electron populations.

The primary origin of electric and magnetic fluctuations, driving radial diffusion, is widely accepted to be ultra-low frequency (ULF) wave activity (Elkington et al., 1999) in the Pc-5 band (1.67–6.67 mHz (Jacobs et al., 1964)). Wave-particle interactions between these ULF waves and radiation belt electrons are particularly effective when the wave frequency is a multiple of the electron drift frequency, constituting a drift-resonant interaction. If interactions with Pc-5 waves continue over a broad frequency range, then the displacement of a particle in L* may evolve stochastically, following continuous interactions with multiple waves, and be described as a diffusive process (Ukhorskiy & Sitnov, 2013; Ukhorskiy et al., 2009). In this diffusive regime, the radial diffusion coefficient, D_{LL}, quantifies the mean square displacement of electrons across L*, and is a measure of the radial diffusion rate.

Analytic expressions describing rates of radial diffusion differ depending on whether the waves can be characterized as electromagnetic or electrostatic in nature. In the former case, the magnetic field variations perturbing particle drifts are accompanied by induced electric fields satisfying Faraday's law, and may be exemplified by Alfvénic fluctuations in the magnetosphere (e.g., Fälthammar, 1965). In the latter case, large-scale variations in the dawn-dusk potential electric field resulting from reconnection processes may drive electrostatic variations (e.g., Cornwall, 1968), similarly perturbing particle orbits based on the effect of the electric field alone. In both cases, expressions may be derived based either on a description of the effect of the perturbing waves on the drift motion of a trapped particle (Fälthammar, 1968; Schulz & Eviatar, 1969; Schulz & Lanzerotti, 1974; Ukhorskiy et al., 2005), or beginning with a Hamiltonian description of the wave-particle interaction (Brizard & Chan, 2001). In the case of electrostatic variations, the appropriate diffusion coefficient may be written as

$$D_{LL}^{ES} = \frac{1}{8B_E^2R_E^2}L^6\sum_m P_m^E\left(L,m\omega_d\right). \quad (1)$$

Here, a particle drifting about the Earth with frequency ω_d will resonantly interact with waves matching the drift resonant condition $\omega = m\omega_d$, where m describes the global azimuthal structure of the waves. In Equation 1, B_E is the Earth's dipole moment, R_E is Earth's radius, and P_m^E is the power spectral density (PSD) of the perturbing electric fields at the resonant frequency. The electrostatic diffusion coefficient (Equation 1) has an explicit L^6 dependence, in addition to any L dependence in the PSD, P_m^E.

If, on the other hand, the particles are interacting with electromagnetic Alfvénic fluctuations (where magnetic and electric perturbations are related by Faraday's law), the radial diffusion coefficient takes the form

$$D_{LL}^{M} = \frac{\mu^2}{8q^2\gamma^2B_E^2R_E^4}L^4\sum_m m^2P_m^B\left(L,m\omega_d\right). \quad (2)$$

In this expression, P_m^B is the PSD of the compressional wave magnetic field at frequency $m\omega_d$, and γ and μ are the relativistic Lorentz factor and first adiabatic invariant, respectively. The L dependence of the electromagnetic diffusion coefficient (Equation 2) is more complicated since γ also depends on L. In the ultra-relativistic limit $\gamma^2 \propto L^{-3}$, so for radiation belt electrons, L^4 / γ^2 is approximately proportional to L^7, not including the L dependence implicit in P_m^B (Elkington et al., 2003).

We note that in the classic "electromagnetic" diffusion formulas given by Fälthammar (1965), the particle perturbations leading to diffusion result from two effects: variations in the magnetic field along the drift orbit, as well as the electric field induced by these magnetic field fluctuations. That is, the particle motion is a result of the Faraday-coupled electric and magnetic field variations along a trajectory. In practice, however, it is difficult to distinguish between the electrostatic variations implied in Equation 1 from the induced electric fields measured in space, leading to the Fei et al. (2006) expression in Equation 2. Perry et al. (2005) showed that the magnetic field phase and the induced electric field phase are not independent. The Faraday-coupled fields, including correct phase, will generally lead to reduced rates of radial diffusion from that given in Equations 1 and 2.

A number of studies have calculated D_{LL} coefficients based on the PSD of ULF waves (e.g., Ali et al., 2015, 2016; Barani et al., 2019; Brautigam & Albert, 2000; Lejosne et al., 2013; Liu et al., 2016; Olifer et al., 2019; Ozeke et al., 2012, 2014), using different data sets and formulations. Several options for D_{LL} coefficients are therefore available. However, a full comparison of how well each available D_{LL} parameterization performs in a diffusion model, both in respect to observations, and to the results from other D_{LL} coefficients, has yet to be determined. This paper is an extension of a previous study (Drozdov, Shprits, Aseev, et al., 2017) in which the sensitivity of long-term simulations, performed with the Versatile Electron Radiation Belt (VERB) code, to both the Brautigam and Albert (2000) and Ozeke et al. (2014) radial diffusion coefficients (D_{LL}), was investigated. Here we consider more recent parameterizations of D_{LL} (Ali et al., 2015, 2016; Liu et al., 2016) and an additional D_{LL} by Brautigam et al. (2005), contrasting the results achieved using these parameterizations to the widely used Brautigam and Albert (2000) and Ozeke et al. (2014) diffusion coefficients.

1.1. Parameterizations of Radial Diffusion Coefficients

The radial diffusion coefficients given by Brautigam and Albert (2000) consist of both an electromagnetic and electrostatic term (denoted here as D_{LL}^{BAEM} and D_{LL}^{BAES}, respectively), following the formalism presented by Fälthammar (1965). A month of in-situ measurements at $L = 6.6$ (Lanzerotti & Morgan, 1973) and 18 days of ground magnetometer measurements at $L = 4$ (Lanzerotti & Morgan, 1973) were used to construct a Kp parameterized D_{LL}^{BAEM} coefficient. Brautigam and Albert (2000) then calculated the electrostatic D_{LL}^{BAES} term following Cornwall (1968), as a linear function of Kp, defined for $1 \leq \text{Kp} \leq 6$. Subsequent work has demonstrated that using D_{LL}^{BAES} alongside D_{LL}^{BAEM} in radiation belt models results in an over-estimation of the electron content in the slot region (K.-C. Kim et al., 2011; Ozeke et al., 2012). We therefore follow the standard convention here (e.g., Glauert et al., 2014) and exclude D_{LL}^{BAES} from this study, using only the electromagnetic component

$$D_{LL}^{BA} \equiv D_{LL}^{BAEM}, \tag{3}$$

where

$$D_{LL}^{BAEM} = L^{10} \cdot 10^{0.506Kp-9.325} \tag{4}$$

in units of day^{-1}.

Ozeke et al. (2014), following the work by Fei et al. (2006), separated the radial diffusion coefficients into two terms: one accounting for the azimuthal electric field D_{LL}^{OE} of the ULF waves, and the other for the waves' compressional magnetic field D_{LL}^{OM}. Collectively, they provide the D_{LL}^{O} coefficient:

$$D_{LL}^{O} = D_{LL}^{OM} + D_{LL}^{OE}. \tag{5}$$

In recent studies, there has been some discussion as to whether it is valid to assume that the azimuthal electric field and the compressional magnetic field are uncorrelated (Lejosne & Kollmann, 2019; Lejosne et al., 2013), a necessary assumption to treat D_{LL}^{OE} and D_{LL}^{OM} separately. However, we do not consider this question further here, and instead focus on how well the Ozeke et al. (2014) D_{LL} is able to reproduce observations. Both D_{LL}^{OM} and D_{LL}^{OE} are parameterized by the Kp index, where the azimuthal electric field PSD values used to determine D_{LL}^{OE} were given by >15 years of ground magnetometer measurements at 7 different L shells. The resulting expression for the electric D_{LL}^{OE} coefficient is

$$D_{LL}^{OE} = L^{8} \cdot 6.62 \cdot 10^{-13} \cdot 10^{-0.0327L^2+0.625L-0.0108Kp^2+0.499Kp} \tag{6}$$

in units of day^{-1}. The D_{LL}^{OM} parameterization was determined from GOES, AMPTE, and THEMIS satellite measurements, and is given as

$$D_{LL}^{OM} = L^{6} \cdot 2.6 \cdot 10^{-8} \cdot 10^{0.217L+0.461Kp} \tag{7}$$

again, in units of day^{-1}. Similar to the Brautigam and Albert (2000) radial diffusion coefficients, the Ozeke et al. (2014) coefficients are also determined for $\text{Kp} \leq 6$.

More recently, Ali et al. (2016) also used the approach of separating the radial diffusion coefficient into terms for the azimuthal electric field and the compressional magnetic field (Brizard & Chan, 2001; Fei et al., 2006)

$$D_{LL}^{A} \equiv D_{LL}^{AM} + D_{LL}^{AE}. \tag{8}$$

The diffusion coefficients given by Ali et al. (2016) were determined using three years of the Van Allen Probe data set, utilizing the Electric Fields and Waves instrument and the Electric and Magnetic Field Instrument Suite. The Kp index was again used to parameterize the magnetic D_{LL}^{AM} and electric D_{LL}^{AE} coefficients, resulting in

$$D_{LL}^{AM} = \exp(-16.253 + 0.225 \cdot Kp \cdot L^{*} + L^{*}) \tag{9}$$

and

$$D_{LL}^{AE} = \exp(-16.951 + 0.181 \cdot Kp \cdot L^{*} + 1.982 \cdot L^{*}) \tag{10}$$

both in given units of days^{-1} for $0 \le Kp \le 5$. Notice that, while the Brautigam and Albert (2000) and Ozeke et al. (2014) parameterizations are in terms of L, the McIlwain L value (McIlwain, 1961), D_{LL}^{A} is explicitly given in terms of L*.

Previously, Ali et al. (2015) constructed a parameterization for the magnetic component of D_{LL} using observations from the magnetometer on board the Combined Release and Radiation Effects Satellite (CRRES). Magnetic wave power was analyzed to derive a fit for the magnetic diffusion coefficient (Ali et al., 2015, Equation 15). The coefficients for this fit were provided in a form of lookup table for different levels of geomagnetic activity. In his postdoctoral thesis, Ali (2016) continued the construction of D_{LL}^{M} as a function of L, Kp, and μ, based on the same data set as Ali et al. (2015), resulting in:

$$D_{LL}^{AM(CRRES)} = \exp(-16.618 + 0.00060104 \cdot \mu + 0.10003 \cdot Kp \cdot L + L) \tag{11}$$

where the units of $D_{LL}^{AM(CRRES)}$ and μ are days^{-1} and MeV/G, respectively. Equation 11 is applicable for $4.0 \le L \le 6.5, 1 \le Kp \le 7, 500 \le \mu \le 5000$ MeV/G, and is similar to Equation 9; however, it provides explicit dependence on μ and is based on observations taken during the previous solar cycle.

Assuming a purely electrostatic field, a parameterization of the electrostatic component of D_{LL} based on CRRES measurements was given by Brautigam et al. (2005). The Electric Field Instrument on board CRRES was used to derive a fit of electric field power spectral as a function L, Kp, and frequency. Based on the formalism presented by Fälthammar (1965), the radial diffusion coefficient can be written as

$$D_{LL}^{E} = \frac{P(f_d, L, Kp)}{8 \cdot R_E^2 \cdot B_{eq}^2} \tag{12}$$

where P is an electric PSD, f_d is drift frequency, R_E is the Earth radius, and B_{eq} is equatorial magnetic field at the corresponding L. Using the azimuthal component of the global electric field from Holzworth and Mozer (1979), Brautigam et al. (2005) derived an expression for P:

$$P(f_d, L, Kp) = a \cdot L^b \cdot \exp(c \cdot Kp) \tag{13}$$

where P is in (mV / m)^2/mHz, and coefficients a, b, and c are given in a lookup table for different values of the drift frequency f_d (Brautigam et al., 2005, Table 3). Following the drift frequency f_d (in mHz) equation from Brautigam et al. (2005), we assume a dipole magnetic field model to obtain the drift frequency formula:

$$f_d = \frac{0.1183 \cdot \mu}{\sqrt{L^4 + 1.2133 \cdot L + \cdot \mu}} \tag{14}$$

where μ is in units of MeV/G. The electrostatic component of radial diffusion coefficient, $D_{LL}^{BE(CRRES)}$, is then given as

$$D_{LL}^{BE(CRRES)} = 2.7818 \cdot 10^{-4} \cdot L^6 \cdot P(f_d, L, Kp) \tag{15}$$

in units of days^{-1}.

The final radial diffusion coefficient considered in this study is given by Liu et al. (2016). Unlike the studies discussed above, Liu et al. (2016) determine only the electric field component from the Fei et al. (2006) approach, arguing that, since the electric component is greater than the magnetic by orders of magnitude, radial diffusion is primarily controlled by the electric component of the ULF wave.

$$D_{LL}^{L} \equiv D_{LL}^{LE}. \tag{16}$$

A similar argument was also discussed by Ozeke et al. (2014) and Ali et al. (2016). Seven years of measurements from the Time History of Events and Macroscale Interactions during Substorms (THEMIS) satellites were used to determine a Kp and μ-dependent expression for D_{LL}^{LE},

$$D_{LL}^{LE} = 1.115 \cdot 10^{-6} \cdot 10^{0.281 \cdot Kp} \cdot L^{8.184} \cdot \mu^{-0.608} \tag{17}$$

in units of day^{-1}. Previously, Ozeke et al. (2014) and Ali et al. (2016) had not identified a μ dependence in the D_{LL}^{LE} coefficient. Brautigam and Albert (2000) did include a μ dependence in D_{LL}^{BAES}; however, the convention to omit D_{LL}^{BAES} and use only D_{LL}^{BAEM} for the Brautigam and Albert (2000) parameterization means that, for the

work presented in this paper, only the coefficients provided by Liu et al. (2016), Ali (2016), and Brautigam et al. (2005) vary with μ.

1.2. Various Assumptions for Derived Radial Diffusion Coefficients

When considering the variety of the available radial diffusion coefficients, it is worth noting the assumptions made and data used for their evaluation. The measurements used by Brautigam and Albert (2000) are very limited, both spatially and temporally. The continuous function for D_{LL}^{BAEM}, extending over $L = 3 - 6.6$, is constructed based on measurements from one month of data at two locations: $L = 4$ and $L = 6.6$. Both Brautigam et al. (2005) and Ali et al. (2016) use several months of CRRES observations. Brautigam et al. (2005) considered the period from January through October 1991, while Ali et al. (2016) utilized a year of measurements, extending from October 1990 until October 1991.

Ozeke et al. (2014) used the longest and most extensive data set. The ground-based measurements included CARISMA (Canadian Array for Real-time Investigations of Magnetic Activity) observations from January 1990 to May 2005, and SAMNET (Sub-Auroral Magnetometer NETwork) observations from 1987 to 2002. These observations involved mapping ULF wave power observed on the ground to a corresponding electric field in space, making a number of assumptions about the spatial structure of the waves, and characterizing all fluctuations observed on the ground as guided Alfvén waves in a pure dipole field. In situ satellite measurements used by Ozeke et al. (2014) included GOES observations from 1996 to 2005, and measurements from 5 THEMIS spacecraft in the range $L = 5$–7 from 2007 to 2011. The authors also indirectly included measurements from AMPTE (Active Magnetospheric Particle Tracers Explorers) by using the figure of PSD presented by Takahashi and Anderson (1992). Liu et al. (2016) also used THEMIS data, taking THEMIS-D measurements from January 2008 to December 2014. The most recent satellite data was used by Ali et al. (2016), who took Van Allen Probes measurements from September 2012 to August 2015.

Observational platforms can themselves influence the calculated PSD. As noted in Ozeke et al. (2014), the high apogee of the THEMIS spacecraft leads to extreme Doppler effects in the inner magnetosphere, causing an over-estimation of the power spectral densities at low-L. For this reason, Ozeke et al. (2014) only considered THEMIS measurements in the $L = 5$–7 range in the validation of their method. THEMIS also suffers from "shorting effects" as it moves into the plasmasphere, causing large DC offsets that can potentially pollute the PSD in the inner magnetosphere unless properly accounted for and removed (Califf & Cully, 2016). Similarly, DC offsets are often observed on THEMIS (which may be attributable to photoelectrons) that vary with spacecraft position; these shifting errors may also contribute to an overestimation of observed power at ULF frequencies (Califf et al., 2014). Additionally, rotational eclipses on THEMIS at dawn and dusk make observations of the azimuthal electric field at these local times difficult, and the lack of information along the THEMIS spin axis affects measurements, when the local magnetic field differs from the mean field-aligned system (Malaspina et al., 2015), can similarly cause significant errors in THEMIS-estimated electric fields used by Liu et al. (2016) if these effects were not properly accounted for.

Ozeke et al. (2014) make assumptions regarding the azimuthal spatial structure of the wave activity, resulting in a potential factor of 4 difference in the PSD mapped from the ground into space. Of particular concern may be the misidentification of Alfvénic waves driven by drift-bounce (Mager & Klimushkin, 2005; Ozeke & Mann, 2001) and other plasma instabilities, which will cause overestimation of the PSD causing diffusion.

Finally, single-point measurements, of necessity, require some assumptions about the azimuthal mode structure of the observed waves. For the D_{LL} estimates provided in all the works under examination here, an $m = 1$ assumption is uniformly made. However, modeling (Elkington et al., 2012; Z. Li et al., 2017; Tu et al., 2012) and observational (Barani et al., 2019; Sarris et al., 2013) studies indicate that significant power may be attributable to larger azimuthal m numbers, causing an overestimation of the power in the $m = 1$ mode.

1.3. Comparison of the Radial Diffusion Coefficients

Figure 1 shows a comparison between different radial diffusion coefficients. Two values of Kp are considered: Kp = 1 for low activity (left panel) and Kp = 5 for active conditions (right panel). For the Ali (2016)

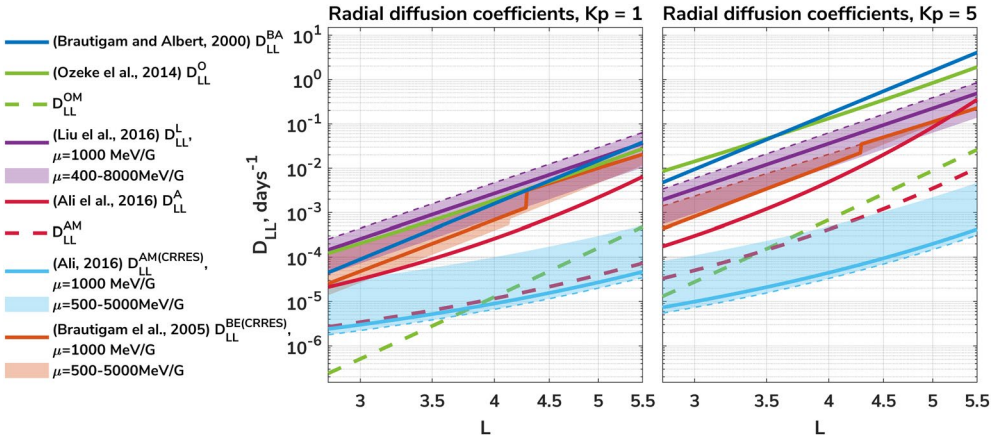

Figure 1. A comparison of various radial diffusion coefficients. We show the electromagnetic D_{LL} from Brautigam and Albert (2000) (dark blue line); magnetic D_{LL} from Ozeke et al. (2014) (green dashed); electric D_{LL} from Ozeke et al. (2014) (green solid line); electric D_{LL} at μ = 1000 MeV/G from Liu et al. (2016) (solid magenta line), as well as the variation of this coefficient for $\mu \in [400, 8000]$ (magenta area); electric D_{LL} from Ali et al. (2016) (red solid line); magnetic D_{LL} from Ali et al. (2016) (red dashed line); magnetic D_{LL} at μ = 1000 MeV/G from Ali (2016) (cyan line), as well as the variation of this coefficient for $\mu \in [500, 5000]$ MeV/G (cyan area); electric D_{LL} at μ = 1000 MeV/G from Brautigam et al. (2005) (orange line), as well as the variation of this coefficient for $\mu \in [500, 5000]$ MeV/G (orange area). When a μ range is given, dashed lines indicate left (lower) boundary of μ range. Left panel corresponds to Kp = 1 and right panel to Kp = 5.

and Brautigam et al. (2005) coefficients, a range of μ values are shown, $\mu \in [500;5000]$ MeV/G, signified by shaded areas. For the Liu et al. (2016) coefficient, the range is $\mu \in [400;8000]$ MeV/G. The range of μ shown is either explicitly prescribed by the model or matches that shown in the associated study. Sudden changes in the Brautigam et al. (2005) coefficient at $L \approx 4.2$ are due to the use of the lookup table in Equation 13.

At both levels of activity, the Ozeke et al. (2014) D_{LL}^{OM}, Ali et al. (2016) D_{LL}^{AM}, and Ali (2016) $D_{LL}^{AM(CRRES)}$ are considerably lower than the D_{LL}^{E} coefficients, indicating that the rate of radial diffusion is primarily governed by the azimuthal electric fields when considered in the Fei et al. (2006) approach. As mentioned above, this observation has been discussed in a number of studies (e.g., Ali et al., 2015, 2016; Z. Li et al., 2016; Ozeke et al., 2014). The coefficients from Brautigam and Albert (2000) D_{LL}^{BA}, Brautigam et al. (2005) $D_{LL}^{BE(CRRES)}$, Ozeke et al. (2014) D_{LL}^{O}, and Liu et al. (2016) D_{LL}^{L} are in close agreement for L = 3–5.5 at Kp = 1. However, at Kp = 5, while D_{LL}^{BA} and D_{LL}^{O} are still comparable, D_{LL}^{L} and $D_{LL}^{BE(CRRES)}$ have not increased as readily. The D_{LL}^{L} and $D_{LL}^{BE(CRRES)}$ coefficients increase with decreasing μ, suggesting that lower energy electrons undergo faster radial diffusion. At Kp = 1, the D_{LL}^{L} values for μ = 400 MeV/G are the largest of all shown, but for Kp = 5, D_{LL}^{L} is less than D_{LL}^{BA} and D_{LL}^{O} over all L and μ. The magnetic radial diffusion coefficient of Ali (2016), $D_{LL}^{AM(CRRES)}$, increases with increasing μ. However, the largest values of the magnetic diffusion coefficient are still lower than the electric diffusion coefficients, given the limits of the fitted domain ($\mu \leq$ 5000 MeV/G).

While a comparison of D_{LL} values is instructive, a better test of the different parameterizations is use in a radiation belt model followed by comparison with observations. In this study, we use the parameterizations of radial diffusion described above in long-term runs of the VERB model and compare results with the Van Allen Probes observations.

2. Methodology

2.1. Data

In this study, we considered two periods. A period nearly from the start of the Van Allen Probes mission (Stratton et al., 2013), spanning from October 1, 2012 to October 1, 2013, and a period from January 2015 to January 1, 2016.

Initial and boundary conditions for the VERB model runs are formed from measurements from Van Allen Probe satellites RBSP-A and RBSP-B, using the Relativistic Electron Proton Telescope (REPT: Baker et al., 2013) and the Magnetic Electron Ion Spectrometer (MagEIS: Blake et al., 2013) instruments. MagEIS measurements are used for < 2.1 MeV and REPT for energies ≥ 2.1 MeV. The twin Van Allen Probes have an orbital period of ~9 h, regularly sampling $L^* \approx 1.2 - 5.5$. Across MagEIS and REPT, electron energies from ~ 30 keV to > ~ 8 MeV can be measured, and the spinning satellite is capable of sampling several pitch angle sectors. To formulate the data-driven boundaries, the measured flux values were binned into 8 hour bins, and by L^* from $L^* = 1$–5.5 in steps of 0.1 L^*. The electron flux is linearly interpolated onto an equatorial pitch angle grid, in steps of 5°, from 0° to 90°.

To illustrate comparisons of the model output with observations, measurements of ~ 1 MeV electrons from the MagEIS detector at an equatorial pitch angle (α_{eq}) of 70° are used. In addition, comparisons at other energies (~ 0.6 MeV from MagIES and 4.2 MeV from REPT) are presented in Supporting Information S1. All equatorial pitch angles and L^* values are calculated with the TS07D magnetic field model (Tsyganenko & Sitnov, 2007). We used the TS07D magnetic field model to obtain both the local and equatorial magnetic fields when calculating the equatorial pitch angles, assuming conservation of the first adiabatic invariant.

2.2. VERB Code

The evolution of electron phase space density in the radiation belts is described by the Fokker-Planck equation (Schulz & Lanzerotti, 1974). Using a single grid approach, the VERB code (Shprits et al., 2015; Subbotin & Shprits, 2009, 2012) computes a numerical solution of the equation:

$$\begin{aligned} \frac{\partial f}{\partial t} = {} & \frac{1}{G}\frac{\partial}{\partial L^*}\bigg|_{V,K} GD_{L^*L^*}\frac{\partial f}{\partial L^*}\bigg|_{V,K} + \\ & \frac{1}{G}\frac{\partial}{\partial V}\bigg|_{L^*,K} G\left(D_{VV}\frac{\partial f}{\partial V}\bigg|_{L^*,K} + D_{VK}\frac{\partial f}{\partial K}\bigg|_{L^*,V}\right) + \\ & \frac{1}{G}\frac{\partial}{\partial K}\bigg|_{L^*,V} G\left(D_{KK}\frac{\partial f}{\partial K}\bigg|_{L^*,V} + D_{VK}\frac{\partial f}{\partial V}\bigg|_{L^*,K}\right) - \frac{f}{\tau_{lc}} \end{aligned} \tag{18}$$

where V is adiabatic invariant, $V \equiv \mu \cdot (K + 0.5)^2$ and $G = -2\pi B_0 R_E^2 \sqrt{8\,\mu \cdot m_0}\,/(K + 0.5)^2/L^{*2}$ is the Jacobian of the transformation from an adiabatic invariant system (μ, J, Φ), B_0 is the field on the equator of the Earth's surface, m_0 is the electron's rest mass. Bounce-averaged diffusion coefficients are denoted by $D_{L^*L^*}, D_{VV}, D_{KK}$ and D_{VK}. A loss term of f/τ_{lc} is included to incorporate losses to the atmosphere and magnetopause, where τ_{lc} represents the electron's lifetime inside the loss cone or outside of the last closed drift shell (LCDS), which was calculated using the TS05 magnetic field model (Tsyganenko & Sitnov, 2005). The lifetime of the particles outside the LCDS is calculated based on their energy and pitch-angle dependent drift period.

V and K are convenient for numerical calculations, because K is independent of particle energy, and V depends only weakly on particle pitch angle. We used the Full Diffusion Code (Ni et al., 2008; Orlova & Shprits, 2011; Shprits & Ni, 2009) to compute bounce-averaged diffusion coefficients in the manner described in previous work by Drozdov, Shprits, Aseev, et al. (2017). Plasmaspheric hiss is included inside the plasmapause using the wave model by Orlova et al. (2014), chorus waves are included on the day and night sides (Orlova et al., 2012), and VLF transmitters and lightning-generated whistlers are included, as described by Subbotin et al. (2011). To accurately simulate multi-MeV electrons, we also included electromagnetic ion cyclotron (EMIC) waves as described by Drozdov, Shprits, Usanova, et al. (2017) due to their defining role in the modeling of high-energy electrons (Drozdov et al., 2020). We used Carpenter and Anderson (1992) to define the plasmapause location. All diffusion coefficients, corresponding to local scattering as well as radial diffusion, are dependent on the Kp-index (except EMIC waves, which are parameterized by solar wind dynamic pressure (see Drozdov, Shprits, Usanova, et al., 2017)). The radial diffusion parameterizations are all also Kp-dependent and are assumed to follow the described Kp trend for all values of Kp.

The 3-D VERB code simulation domain extends from $L^* = 1$ to $L^* = 5.5$, and encompasses electron energies from 10 keV to 10 MeV at $L^* = 5.5$. Equatorial pitch angles from 0.7° to 89.3° are covered, and the grid in the L^*, V, K space has dimensions of $46 \times 100 \times 101$. To define the calculation box, boundary conditions are required at the minimum and maximum values of these three variables. The lower V boundary is defined as constant phase space density, representing the average source population, and the upper boundary is set to zero due to the absence of high-energy electrons. The lower K boundary also set to zero, representing the losses to the atmosphere in the loss cone. The upper K boundary is defined as zero derivative. For the inner L^* boundary, at $L^* = 1$, the phase space density is zero, capturing loss to the atmosphere. The outer L^* is set from the Van Allen Probes data, as described in Section 2.1, and is updated every 8 h during the run. During the times when LCDS crosses the simulation domain, the outer L^* boundary is updated every timestep and is modified to account for exponential loss of the electrons (on the scale of drift period) due to magnetopause shadowing. The Van Allen Probes flux is converted to phase space density, the logarithm of which is interpolated to the V and K simulation grid. However, Van Allen Probes measurements do not cover the full range of V and K. For V and K values not observed by the Van Allen Probes, we create a synthetic phase space density array, assuming a sine pitch angle distribution and an average energy spectra. This array is normalized to a valid measurement as close as possible to 1 MeV, $\alpha_{eq} = 75°$. Thus, two 2D arrays are created: the interpolated phase space density from the Van Allen Probe observations and the synthetic normalized phase space density array. All data gaps in the first array are replaced with the values from the second. The initial condition is created from the Van Allen Probes data in a similar fashion, but for each L^* bin rather than for each time, using a steady-state solution for the synthetic array. All 2-D slices of the outer boundary condition and each L^* slice of the initial condition are visually inspected for interpolation artifacts.

The VERB code is used for both 1-D (VERB-1D) and 3-D (VERB-3D) simulations. In the case of the 1-D simulation, where energy and pitch angle diffusion are omitted, Equation 18 simplifies to:

$$\frac{\partial f}{\partial t} = \frac{1}{G}\frac{\partial}{\partial L^*}\bigg|_{V,K} GD_{L^*L^*}\frac{\partial f}{\partial L^*}\bigg|_{V,K} - \frac{f}{\tau} \tag{19}$$

where τ has been modified to now be the lifetime of the electrons, representing the loss resulting from pitch angle diffusion. The electron lifetimes due to the hiss waves inside plasmasphere are calculated following Orlova et al. (2016), and due to the chorus waves outside of the plasmasphere following Gu et al. (2012). Both of those electron lifetime parameterizations are derived with limitation of the energy range. While the energy coverage is substantial, there are points with undefined electron lifetimes. We fill this energy gap by assuming lifetimes of 6/Kp outside the plasmasphere and 10 days inside, similar to the previous studies (e.g., Drozdov, Shprits, Aseev, et al., 2017; Ozeke et al., 2014; Shprits et al., 2006). VERB-1D requires boundary conditions at the inner and outer L^* boundaries, again set at $L^* = 1$ and 5.5, respectively. As for VERB-3D, the phase space density at $L^* = 1$ is set to zero, and at $L^* = 5.5$ is set by Van Allen Probe measurements. The initial condition is again set from Van Allen Probe observations.

For the simulations using the D_{LL}^L parameterization for radial diffusion, we require the D_{LL}^L coefficient for $\mu < 400$ MeV/G, owing to the described grid setup for VERB. Liu et al. (2016) caution using D_{LL}^L for $\mu <$ 400 MeV/G, as they found that the D_{LL} data showed less agreement with their parameterization over this μ range. Here, we use the D_{LL}^L value at $\mu = 400$ MeV/G for $\mu < 400$ MeV/G, effectively holding D_{LL}^L constant with μ for $\mu < 400$ MeV/G. In Section 4.2, we discuss the impact of this choice further and explore various other approaches.

2.3. Normalized Difference

To quantify the agreement between model output and Van Allen Probes observations, we use the normalized difference (ND) of the electron flux (j):

$$ND(L^*,t) = \frac{j_{obs}(L^*,t) - j_{model}(L^*,t)}{\max\limits_{over\ L^*\ at\ const\ t} \frac{j_{obj}(L^*,t) + j_{model}(L^*,t)}{2}} \tag{20}$$

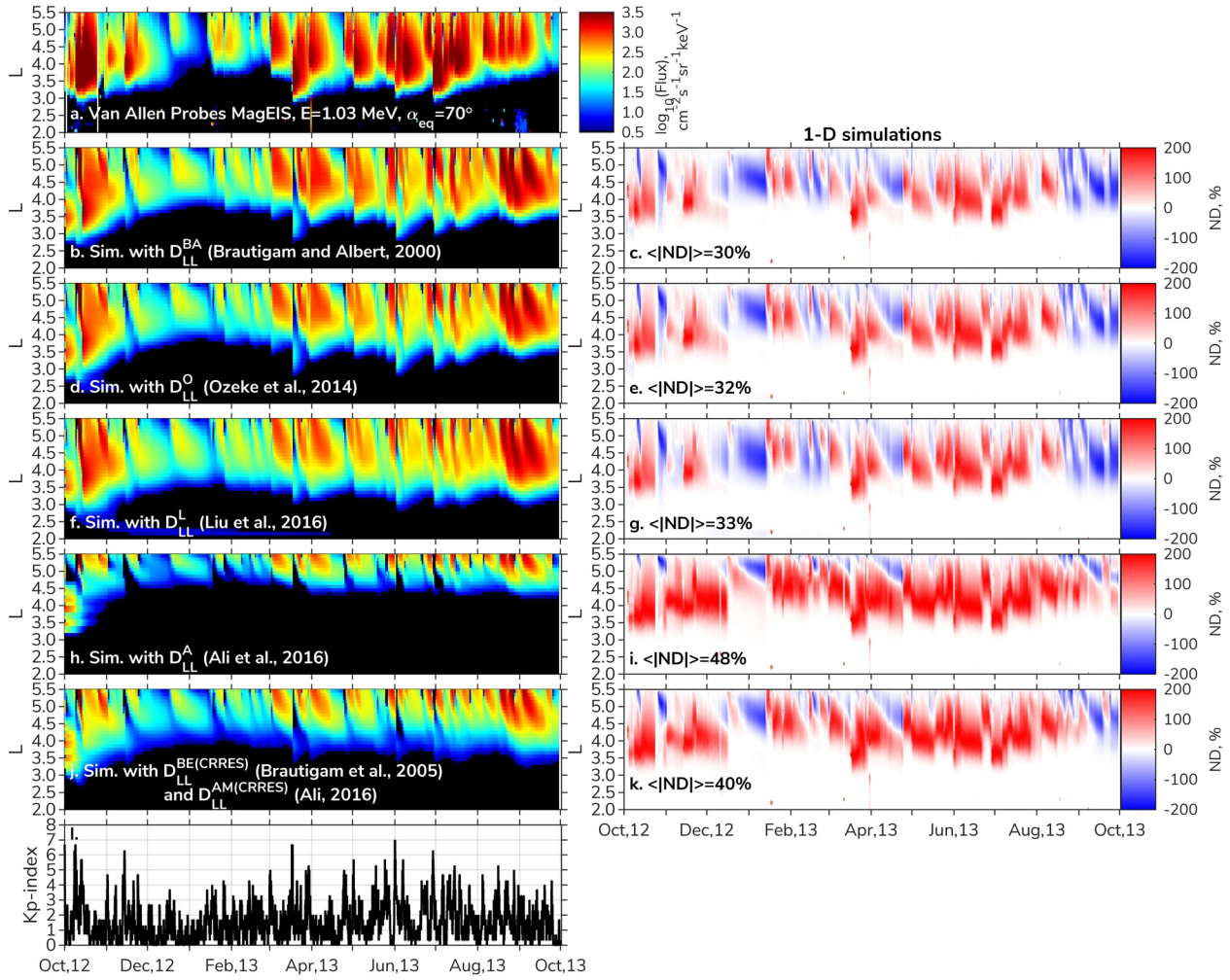

Figure 2. (a) Measurements of electron flux at 1.03 MeV, at pitch angle $\alpha_{eq} = 70°$ from Van Allen Probes Magnetic Electron Ion Spectrometer (MagEIS) instrument; (b, d, f, h, and j) 1-D Versatile Electron Radiation Belt (VERB) code simulation with ($D_{LL}^{BA}, D_{LL}^{O}, D_{LL}^{A}, D_{LL}^{L}$), and $D_{LL}^{BE(CRRES)} + D_{LL}^{AM(CRRES)}$ respectively; (c , e, g, i, and k) normalized difference between simulations and measurements, corresponding with the mean absolute value. (l) Kp-index.

This metric has been used previously by Subbotin and Shprits (2009), Drozdov, Shprits, Aseev, et al. (2017) and Wang et al. (2020) and provides the difference between observations (j_{obs}) and model output (j_{model}) at a particular energy, L^*, α_{eq}, and time. The result is normalized by the maximum flux in the heart of the belt and is therefore particularly useful to determine how well the simulation reproduces the observed flux peaks, as well as the behavior around the maximum. To compute the normalized difference, the Van Allen Probes data is averaged over a 12-hour period and binned by L^* in steps of 0.1 L^*. We exclude points at $L^* \leq 2$ due to the negligible contribution of the radial diffusion on the electron flux dynamics at low L^*.

3. Modeling and Comparison With Observation

3.1. 1-D Simulations With Realistic Boundary Conditions

Figure 2 shows 1.03 MeV, $\alpha_{eq} = 70°$ MagEIS observations (panel a) alongside the corresponding output from four 1-D simulations with data-driven boundary conditions, each using different D_{LL} coefficients (panels b, d, f, h, and g). Normalized differences between each simulation and the observations are also included (c, e, g, and i), and the absolute mean of the normalized difference shown on each plot for reference. As seen in Figure 2j, the one-year period covers various Kp-index levels, incorporating a range of geomagnetic changes.

With an exception of the simulations with D_{LL}^{A}, the 1-D modeled simulations flux generally reproduces the observed flux variation. In particular, the L^{*} location of the inner edge of the outer belt shows closest agreement with data for the D_{LL}^{BA}, D_{LL}^{O} or D_{LL}^{L} coefficients. However, the modeled 4.2 MeV flux (see Figure S2) indicates noticeable underestimation. We attribute this to the absence of local acceleration from chorus waves, which has been shown to largely impact the dynamics of the ~ MeV population (e.g., Allison et al., 2021; Horne et al., 2005; Thorne et al., 2013).

When using the D_{LL}^{A} coefficient, VERB-1D shows a lower flux at 1.03 MeV than observed. Examining Figure 1, it can be seen that the electric component of D_{LL}^{A} is lower than the equivalent electric component from either D_{LL}^{O} or D_{LL}^{L} for both Kp = 1 and Kp = 5. This variation yields largely different behavior to the other VERB-1D runs, with the outer radiation belt remaining at $L^{*} > 4$ for the entirety of the October 2012 to October 2013 period.

The final VERB-1D simulation, shown in Figure 2j, uses both the Ali (2016) and Brautigam et al. (2005) parameterizations. In doing so, D_{LL} coefficients are provided that are built solely on CRRES measurements, taken during the previous solar cycle. However, Ali (2016) follows the Fei et al. (2006) formalism, and accounts for only the magnetic component of the ULF wave field, while Brautigam et al. (2005) provides the radial diffusion coefficient arising from electrostatic fluctuations. As a result, the electric component of the ULF waves is not explicitly included; however, ULF wave electric fields may be partially counted in the PSD measurements utilized by Brautigam et al. (2005) when deriving their electrostatic diffusion coefficients. A comparison between the model output, shown in panel j, and the Van Allen Probes observations reveals a larger underestimation in the 1 MeV electron flux than when the D_{LL}^{BA}, D_{LL}^{O} and D_{LL}^{L} coefficients were used. The missing ULF wave electric component may help account for this discrepancy.

3.2. 3-D Simulations Including Local Diffusion Processes

Local acceleration from chorus waves can act to produce larger flux enhancements than radial diffusion alone. However, as the direction of radial diffusion and, in part, the rate of diffusion, are governed by the gradients in phase space density, to which local acceleration and scattering contribute, it is important to include these processes when evaluating the various radial diffusion coefficients. In this section, we use VERB-3D and include local diffusion processes, as described in Section 2.2.

Figure 3 takes the same format as Figure 2. The 3-D simulations for 1.03 MeV, $\alpha_{eq} = 70°$, using each of the four radial diffusion coefficients, are shown (panels b, d, f, h, and j). Alongside each run, the respective normalized difference between the model output and MagEIS observations has again been included (panels c, e, f, g, and k) and the absolute mean of the normalized difference is stated on each plot. In general, electron flux levels are higher for the VERB-3D runs than VERB-1D and show closer agreement with observations.

There is a tendency for the over- or underestimations of each of the model runs to occur across the same periods, albeit covering different L^{*} ranges. For example, regardless of the radial diffusion parameterization used, the model tends to overestimate the 1 MeV flux (for at least part of the outer radiation belt) between December 2012 and January 2013. Empirical models of D_{LL} can differ significantly from those derived using the event-specific values of the measured global ULF wave power (Murphy et al., 2016; Ozeke et al., 2020). As such, differences between the empirical Kp-dependent values and the real global ULF wave-power may have produced some of these over- or underestimations. Despite the over- and underestimations of the flux, when using D_{LL}^{BA}, D_{LL}^{O}, D_{LL}^{L}, or $D_{LL}^{BE(CRRES)} + D_{LL}^{AM(CRRES)}$, the structure of the outer radiation belt has been generally reproduced. In particular, as was the case in the 1-D simulations, the L^{*} extent of the outer belt largely agrees with observations for the runs using D_{LL}^{BA}, D_{LL}^{O} or D_{LL}^{L}. The inclusion of energy and pitch angle scattering has reduced the model flux in the observed slot region and, as a result, the inner edge of the outer belt in the 3-D model run using $D_{LL}^{BE(CRRES)} + D_{LL}^{AM(CRRES)}$ shows a closer match with observations than the corresponding output from VERB-1D. Generally, radial diffusion smooth out peaks in phase space density created by energy diffusion (Shprits et al., 2008). This feedback mechanism can explain why 3-D simulations can reproduce long-term dynamics of the radiation belts, even if radial diffusion processes are quantified differently.

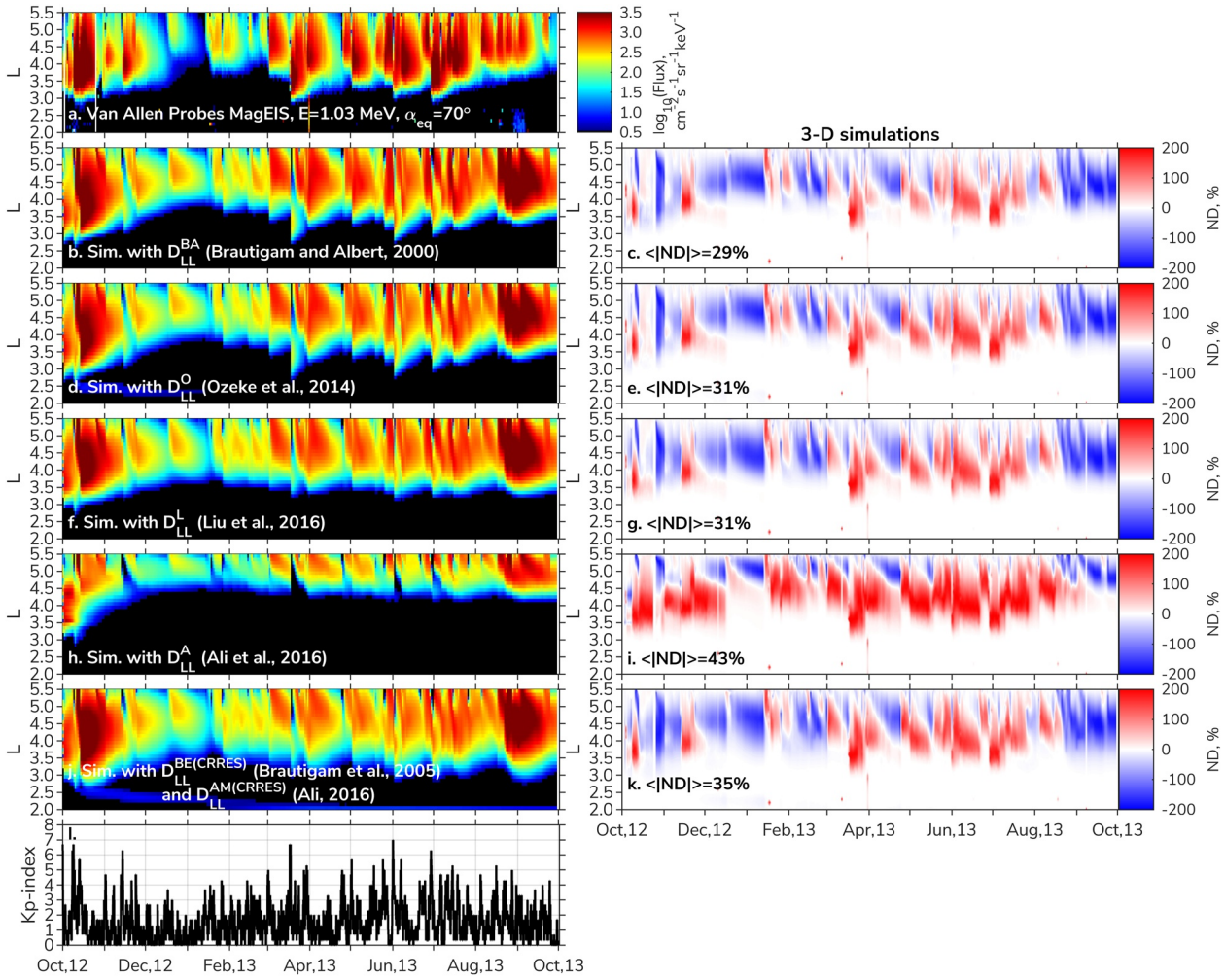

Figure 3. (a) Measurements of electron flux at 1.03 MeV, at pitch angle $\alpha_{eq} = 70°$ from Van Allen Probes Magnetic Electron Ion Spectrometer (MagEIS) instrument; (b, d, f, h, and j) 3-D Versatile Electron Radiation Belt (VERB) code simulation with ($D_{LL}^{BA}, D_{LL}^{O}, D_{LL}^{A}, D_{LL}^{L}$), and $D_{LL}^{BE(CRRES)} + D_{LL}^{AM(CRRES)}$ respectively; (c, e, g, i, and k) normalized difference between simulations and measurements, and the corresponding mean absolute values. (l) Kp-index.

However, as was the case in Figure 2, the simulation with D_{LL}^{A} significantly underestimates the observed fluxes for $L^{*} < 4$. Although the modeled flux is now higher than the 1-D case, the MagEIS flux is still higher than the model output. The inclusion of locally produced peaks in phase space density aids the simulation using D_{LL}^{A}; however, the additional diffusion is not sufficient to fully reproduce the radiation belt dynamics.

3.3. Results of the Simulations at Different Energies

The VERB code simulations are performed for a range of energies. Similar to Figures 2 and 3, Figures S1–S4 show the comparison between observations and various simulations at energies of ~ 600 keV and 4.2 MeV. Figure 4 shows how the averaged absolute normalized difference changes with electron energy. Generally, the difference between simulations and observations is similar at different energies. The average $|ND|$ across all energies, presented in Figure 4, for the 3-D simulations with corresponding diffusion coefficients are 32% (D_{LL}^{BA}), 33% (D_{LL}^{O}), 40% (D_{LL}^{A}), 33% (D_{LL}^{L}), and 36% ($D_{LL}^{BE(CRESS)} + D_{LL}^{AM(CRESS)}$). The simulation with D_{LL}^{BA} results in the smallest average normalized difference and typically provides the closest agreement with observations across different energies. Also, the difference between using various D_{LL} parameterizations in the simulations is less pronounced in 3-D case, in comparison to 1-D. We attribute this to the feedback between the wave-induced changes (additional acceleration and loss mechanisms) and radial transport

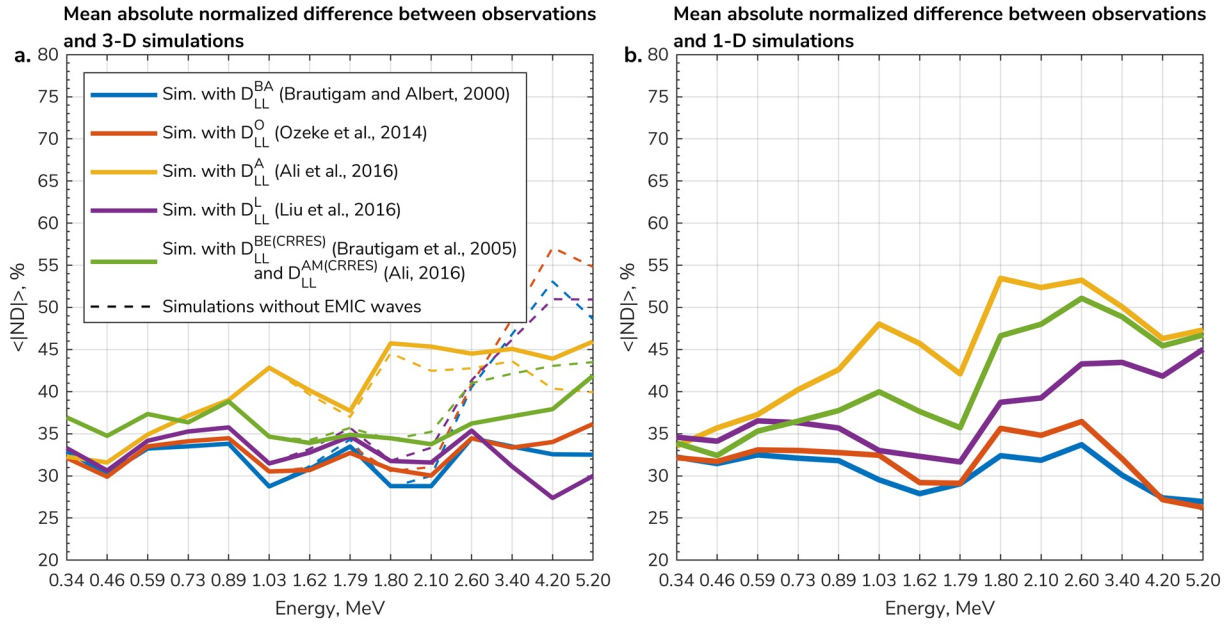

Figure 4. (a) Averaged absolute normalized difference between 3-D simulations and observations at different energies. Different solid colors correspond to different radial diffusion parameterizations according to the legend. Dashed lines correspond to the simulations without electromagnetic ion cyclotron (EMIC) waves. (b) Same as panel (a) but for 1-D simulations.

that minimize the resulting differences in the VERB-3D code solution. Note that we also perform the simulations with and without EMIC waves to explore how the simulations with different radial diffusion parameterization perform at high multi-MeV energies, where the effect of the hiss and chorus waves could be less pronounced (e.g., Ripoll et al., 2016). The simulations without EMIC result in larger error for all simulations, except for the one with D_{LL}^{A}, likely because D_{LL}^{A} provides insufficient radial diffusion, and the additional EMIC loss results in a worse comparison.

4. Discussion

4.1. Underestimation With D_{LL}^{A}

Our simulation results suggest that using D_{LL}^{A} in either VERB-1D or VERB-3D for the selected period significantly underestimates the observations due to insufficient radial diffusion. This parameterization employs the most recent Van Allen Probes observations. The Van Allen Probes mission has covered a relatively inactive period, with few large storms. Perhaps, as a result, the statistics for each Kp level are biased toward lower ULF wave activity. Additionally, it is the only radial diffusion coefficient used here which is only constructed for Kp < 5. The other radial diffusion parameterizations are defined up to at least Kp = 6. During quieter periods, radial diffusion rates are slower, and large changes in the L^{*} value of electron populations are generally achieved during storm periods (e.g., Jaynes et al., 2018; Z. Li et al., 2016; Ukhorskiy et al., 2009). Underestimating the contribution of radial diffusion during high-Kp periods is therefore likely to also impact the difference between model and observations in the following quieter times. During the active time, the rapid high-energy injection may also contribute to the enhancement of the radiation belt flux (e.g., H.-J. Kim et al., 2021). However, the role of such injections in the radiation belt dynamics is yet to be determined.

Another possible reason for the lower radial diffusion rates is that Ali et al. (2016) used the geometric mean (which, in their case, is close to the median value) of PSD for both electric and magnetic field spectra (see Figure 2, Ali et al., 2016). This choice was made due to the nature of the data, since the mean value of PSD does not represent the central tendency in the log-normal distribution that characterizes ULF PSD distributions. An arithmetic mean (i.e., average) of a log-normal distribution, as was used by Ozeke et al. (2014) and Liu et al. (2016), will tend to overestimate the true central tendency. However, the influence of ULF waves

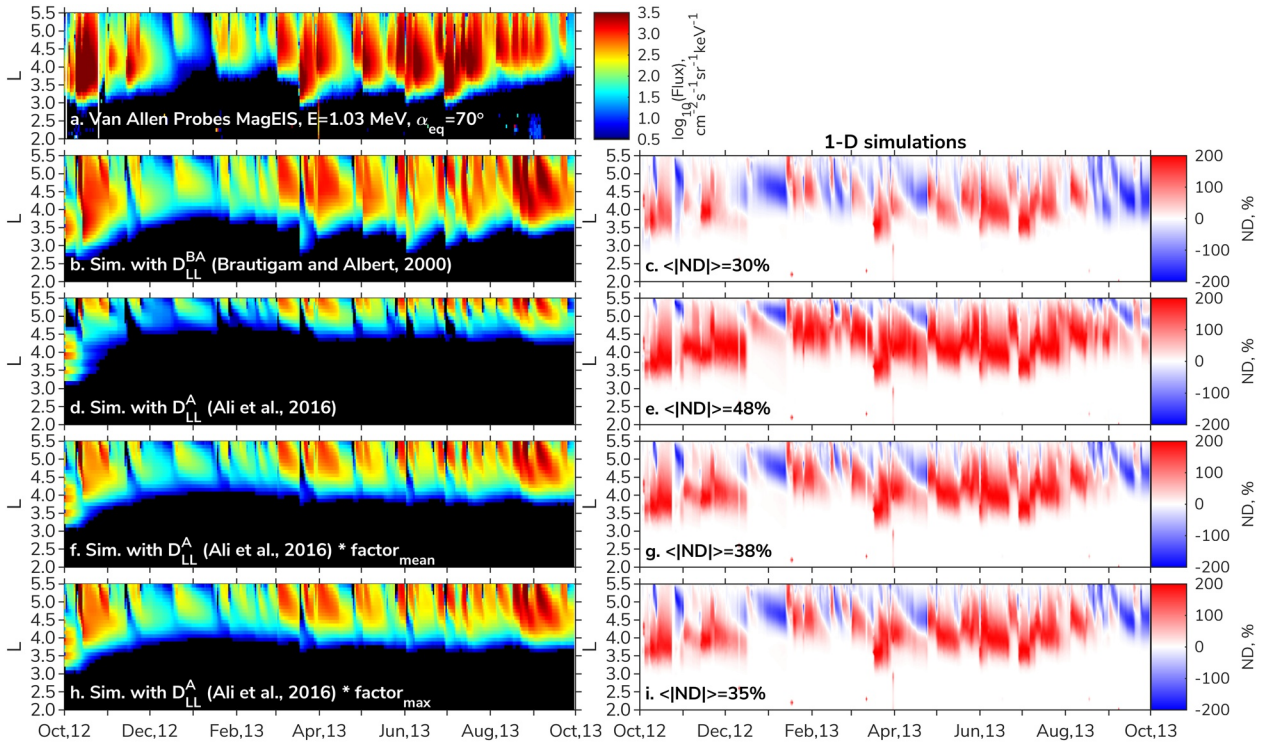

Figure 5. (a) Measurements of electron flux at 1.03 MeV, at pitch angle $\alpha_{eq} = 70°$ from Van Allen Probes Magnetic Electron Ion Spectrometer (MagEIS) instrument; (b, d, f, and h) 1-D Versatile Electron Radiation Belt (VERB) code simulation with (D_{LL}^{BA}, D_{LL}^{A}, $D_{LL}^{A} \cdot \text{factor}_{\text{mean}}$, $D_{LL}^{A} \cdot \text{factor}_{\text{mean}}$) respectively; (c, e, g, and i) normalized difference between simulations and measurements, and corresponding with the mean absolute value.

on electrons is usually considered as the averaged effect of the wave-particle interaction. Also, the radial diffusion coefficient is lineally dependent on PSD (e.g., Equation 12). In an attempt to reproduce how the radial diffusion coefficient would have appeared if the mean of the PSD had instead been used, we employ a scaling factor. This approach is used purely as an illustrative estimate. As a scaling factor, we obtain the ratio between mean and median values presented in Figure 2 from Ali et al. (2016). Since the ratio between mean and median PSD varies over frequency, we simplify the factor by taking the average or maximum values of the ratio. The average (factor$_{\text{mean}}$) and maximum (factor$_{\text{max}}$) values of the ratio are 3.8 and 5.0 for electric field spectra and 3.1 and 5.3 for magnetic field spectra, respectively.

Figures 5 and 6 show the result of 1-D and 3-D simulations with the scaled D_{LL}^{A} coefficients alongside simulations with unchanged D_{LL}^{A} and D_{LL}^{BA}, for reference. In both the 1-D and 3-D cases, the results of the simulation with a scaling factor provide better agreement with observations. The lower boundary of the radiation belt propagates further inward in comparison to the simulation with the unmodified coefficient. In 3-D simulations, the electron flux in the heart of the radiation belts ($L \sim 4 - 5$) is within an order of magnitude of the observations. The mean absolute value of normalized difference also indicates an improvement in the agreement with observations. These results highlight the difficulties in formulating a statistical picture of the PSD for calculating radial diffusion coefficients, as the PSD of ULF waves, similar to whistler waves (e.g., Watt et al., 2017), does not obey a Gaussian nature (Bentley et al., 2018).

To reproduce the Van Allen Probes flux observations using the unmodified D_{LL}^{A} coefficients, additional local acceleration or reduced loss is required. We have assumed here that the loss rates and the pitch angle and energy diffusion coefficients fully capture the extent of the wave-particle interactions. Changes in the rate of local acceleration and scattering alters the gradients in phase space density and therefore also impact how the electron populations diffuse across L^{*}. We argue that, given that the other D_{LL} parameterizations show better agreement with observations, the local wave particle interactions are adequately captured here.

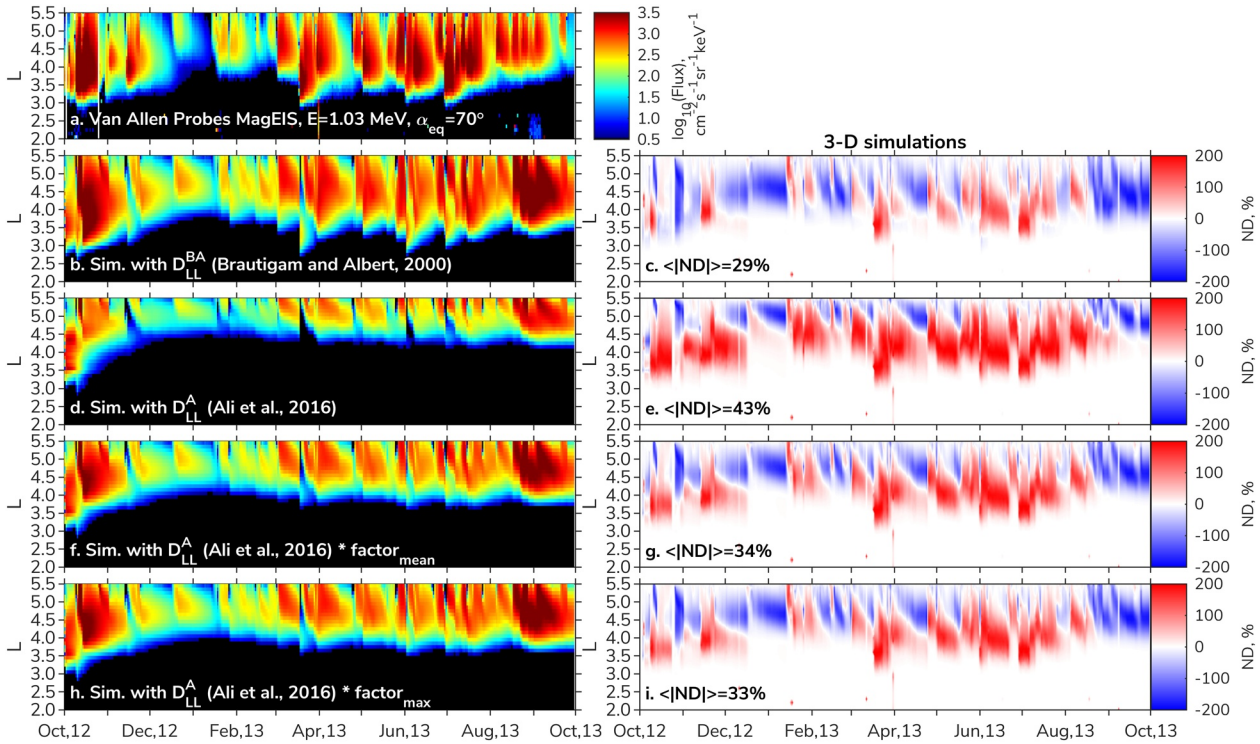

Figure 6. (a) Measurements of electron flux at 1.03 MeV, at pitch angle $\alpha = 70°$ from Van Allen Probes Magnetic Electron Ion Spectrometer (MagEIS) instrument; (b, d, f, and h) 3-D Versatile Electron Radiation Belt (VERB) code simulation with ($D_{LL}^{BA}, D_{LL}^{A}, D_{LL}^{A} \cdot \text{factor}_{\text{mean}}, D_{LL}^{A} \cdot \text{factor}_{\text{mean}}$) respectively; (c, e, g, and i) normalized difference between simulations and measurements, and corresponding with the mean absolute value.

Recent work by Tu et al. (2019) has used the magnetic radial diffusion from the Ali et al. (2016) parameterization, together with the electric radial diffusion coefficient from Liu et al. (2016) to study the June 2015 dropout event. However, as can be seen in Figure 1, the magnetic component of D_{LL} from Ali et al. (2016) is more than an order of magnitude less than the Liu et al. (2016) electric diffusion coefficient. Therefore, the evolution of the radial structure of radiation belt is largely dominated by the Liu et al. (2016) D_{LL} alone. Tu et al. (2019) also compared to model results achieved using the Brautigam and Albert (2000) D_{LL} coefficient for this event and observed differences between the two simulation outputs, with the results from the combined D_{LL}^{L} and D_{LL}^{AM} showing closer agreement with measurements. Their simulations used a larger value of L_{max}^{*} than those shown in this paper, as they did not use a data-driven outer boundary condition. Including a broader L^{*} range in the model may also alter how the outputs using the different D_{LL} coefficients compare to one another, as each parameterization varies across L^{*} differently (see Figure 1). One should also be mindful of the L^{*} (or L) range over which the diffusion coefficient is defined.

4.2. "Energy" Dependence of D_{LL}^{L}

As discussed in Section 1.1, the Liu et al. (2016) electric parameterization and Brautigam et al. (2005) electic parameterization include a μ dependence. In the other studies, the μ dependence of the electric component of D_{LL} has not been included, as the drift-averaged PSD of the ULF waves was taken to be frequency-independent. In the case of the Brautigam and Albert (2000) coefficient, we have neglected the electrostatic term containing μ.

Liu et al. (2016) found that the root-mean-square errors of their fitted D_{LL} increased substantially for $\mu < 400$ MeV/G and, as a result, use of the resulting D_{LL}^{L} coefficients is therefore cautioned for $\mu < 400$ MeV/G. For VERB-3D, we hold the D_{LL} value constant at $\mu = 400$ MeV/G for $\mu < 400$ MeV/G.

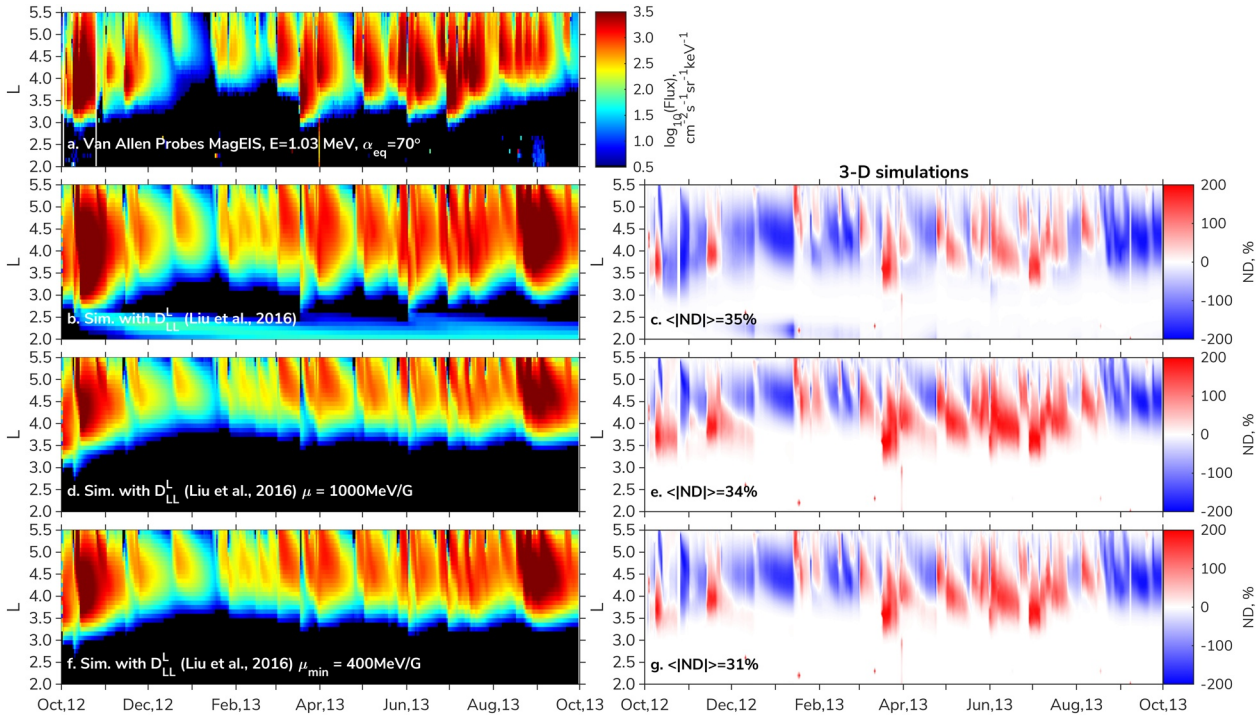

Figure 7. (a) Measurements of electron flux at 1.03 MeV, at pitch angle $\alpha_{eq} = 70°$ from Van Allen Probes Magnetic Electron Ion Spectrometer (MagEIS) instrument. (b) 3-D simulation with $D_{LL}^{L}(Kp, \mu)$, (d) with $D_{LL}^{L}(kp, \mu_0)$, where $\mu_0 = 1000\ MeV\ /\ G$, (f) with $D_{LL}^{L}(kp, \mu_{min})$, where $\mu_{min} \geq 400\ MeV\ /\ G$. (c, e, and g) Normalized difference between simulations on panels (c, d, and f) and measurements, and corresponding to the mean absolute value.

However, an alternative approach is to allow the D_{LL}^{L} to obey the given μ dependence regardless of the μ value, ignoring the caution given. Figure 7b shows the result of this approach.

In contrast with the results from holding D_{LL}^{L} constant with μ for $\mu < 400$ MeV/G (also shown in Figure 7f), the 3-D simulation using the unlimited D_{LL}^{L} produces higher flux peaks for $L^{*} \sim 4$, considering the normalized difference (Figure 7c). Additionally, a remnant belt between $2 < L^{*} < 2.5$ has also been produced that is not observed by the Van Allen Probe. Overestimation of the electron flux now extends over a broader L^{*} range than previously.

Another approach is to ignore the μ dependence of D_{LL}^{L} entirely, and therefore bring the parameterization in line with the other radial diffusion coefficients considered in this paper. Here, we also explore this with the 3-D model. D_{LL}^{L} is set by $\mu = 1000$ MeV/G and then assumed to be μ-independent. Figure 7d shows the resulting flux at 1.03 MeV, $\alpha_{eq} = 70°$. The modeled flux is lower than the output shown in both Figures 7b and 7f, and the outer radiation belt extends over a smaller L^{*} range. Examination of the normalized difference (Figure 7e) reveals larger underestimations in comparison to data.

Including the μ dependence of D_{LL}^{L} improves the agreement between the VERB model output and observations. However, we reiterate the point made by Liu et al. (2016), that the D_{LL}^{L} for $\mu < 400$ MeV/G should be handled carefully, as our simulations show that this can significantly impact the model output, resulting in larger flux values and a remnant belt structure.

4.3. Pitch-Angle Dependence

Due to the electron azimuthal drift period depending on the its equatorial pitch angle, the radial diffusion coefficients may also show pitch angle dependence. Schulz and Lanzerotti (1974) explore the pitch-angle

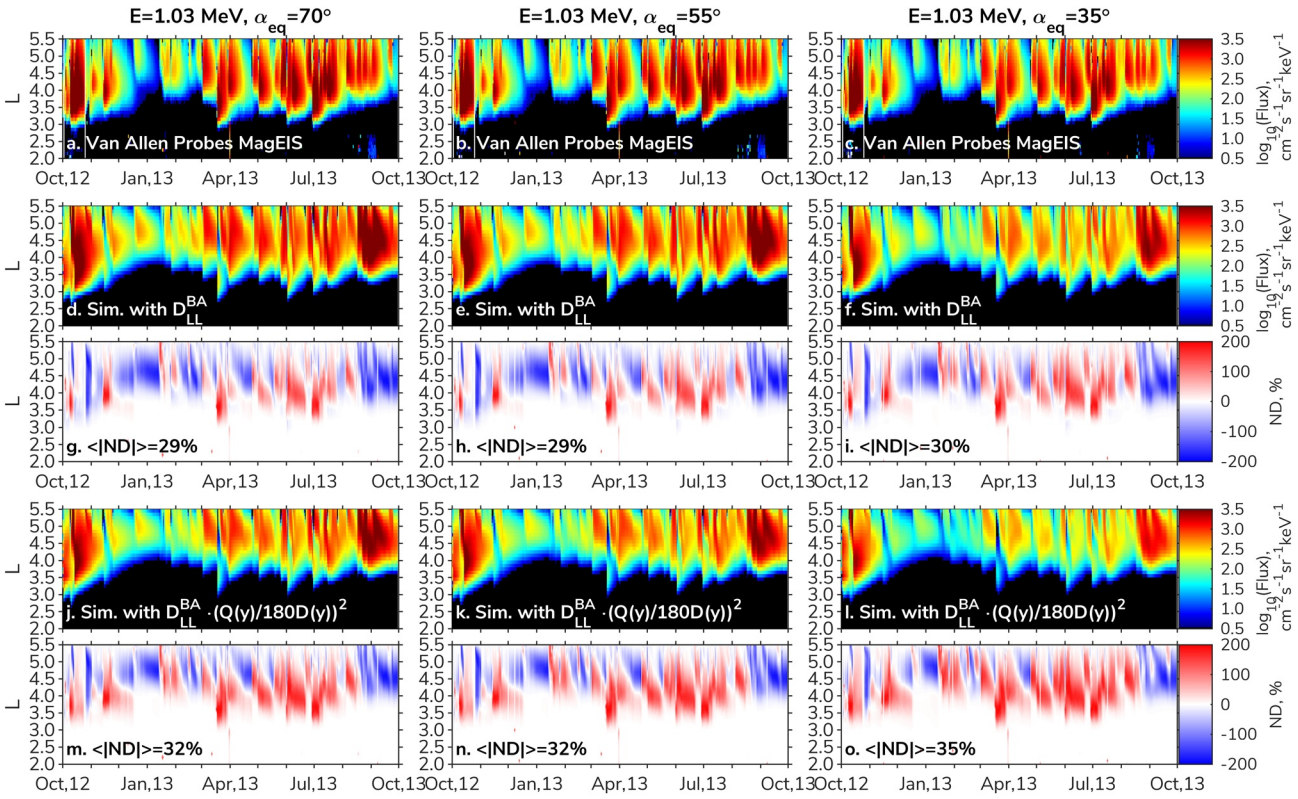

Figure 8. (a–c) Measurements of electron flux at 1.03 MeV, at equatorial pitch angles α_{eq} = 70°,55°,35° from Van Allen Probes Magnetic Electron Ion Spectrometer (MagEIS) instrument; (d, e, and f) 3-D simulation with D_{LL}^{BA} at the same energy and pitch angle as in panels (a–c); (g–i) Normalized difference between simulations on panels (d–f) and measurements, and corresponding to the mean absolute value; (j–l) Similar to panels (d–f) but for 3-D simulations with $D_{LL}^{BA}\cdot(Q(y)/180D(y))^2$; (g–i) Similar to panels (g–i) but for the simulations on panels (j–l) and measurements.

dependency of D_{LL}^{M} coefficient, considering the contribution of step-like impulses in the magnetic field. Schulz (1991) provides the dependence as

$$D_{LL}^{M}(L,y) \sim D_{LL}^{M}(L)\cdot\left(\frac{Q(y)}{180D(y)}\right)^2 \tag{21}$$

where $y = \sin(\alpha_{eq})$, $Q(y)$ and $D(y)$ are auxiliary functions that can be expressed as:

$$Q(y) \approx -27.12667 - 45.39913y^4 + 5.88256y^8 \tag{22}$$

$$D(y) \approx \frac{1}{12}\cdot\left(5.520692 - 2.357194y + 1.279385y^{3/4}\right) \tag{23}$$

Schulz and Lanzerotti (1974) also explore the pitch-angle dependency of the D_{LL}^{ES} coefficient, which represents the contribution from exponentially decaying impulses in the electrostatic field, and conclude that D_{LL}^{ES} is relatively insensitive to the equatorial pitch angle. For the diffusion coefficients considered in this paper, the pitch-angle scaling factor given by Equation 21 can be applied to D_{LL}^{BA}, as its derivation follows the Fälthammar (1965) methodology, consistent with Schulz and Lanzerotti (1974). This approach is taken by Miyoshi et al. (2006) who modeled the October 2001 storm. W. Li et al. (2016) also used the pitch-angle dependence in Equation 21, applying the scaling to the sum of the magnetic D_{LL}^{OM} and electric D_{LL}^{OE} Ozeke et al. (2014) coefficients given by derived using the Fei et al. (2006) formalism. Whether Equation 21 is applicable to diffusion coefficients calculated with the Fei et al. (2006) formalism is unclear.

We explore the effect of pitch-angle dependence given by Equation 21 in the simulations with D_{LL}^{BA}. Figure 8 shows ~1 MeV electron flux at different pitch angles (α_{eq} = 70°,55°,35°) obtained for the observations, sim-

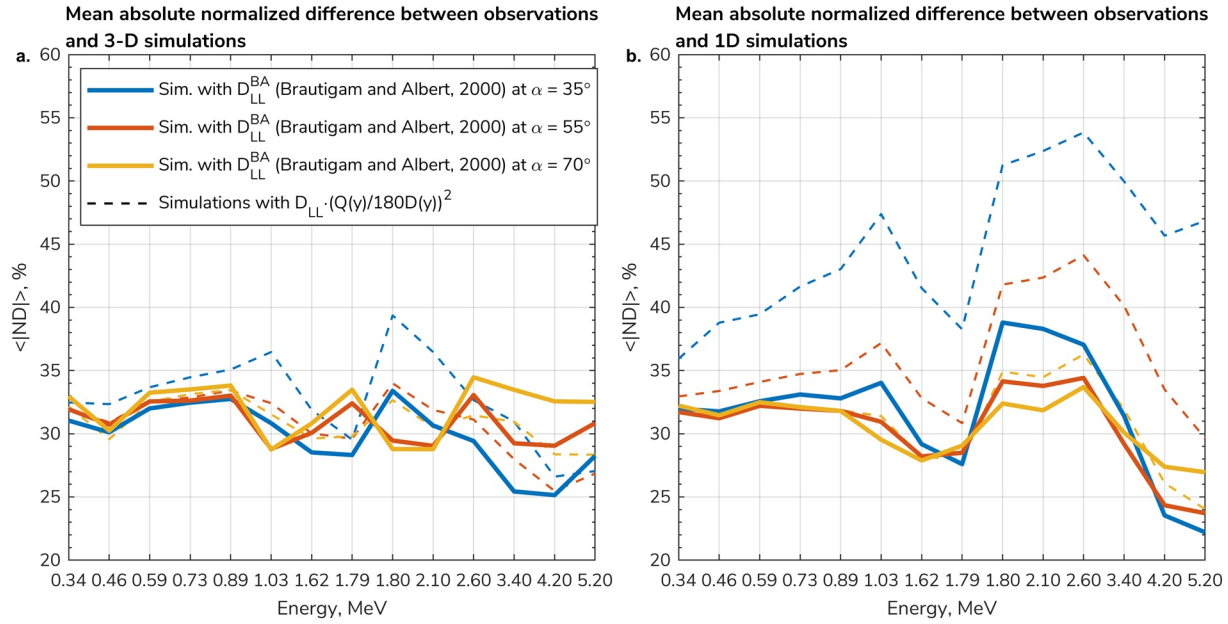

Figure 9. (a) Averaged absolute normalized difference between 3-D simulations and observations at different energies. Solid lines correspond to simulations with D_{LL}^{BA} and dashed lines to the simulation with $D_{LL}^{BA}\cdot(Q(y)/180D(y))^2$. Different colors correspond to different pitch-angles according to the legend. (b) Same as panel (a) but for 1-D simulations.

ulations without pitch-angle dependence, and simulations with pitch-angle dependence and corresponded normalized difference. The pitch-angle dependence alters the results of the 3-D simulations, slightly increasing the difference with observations. Figure 9 shows that a similar trend is also observed at other energies. For the 1-D simulations, imposing a pitch-angle dependence on the radial diffusion coefficient results in a larger increase in the mean normalized difference than for the 3-D simulations (see Figure S5). These results indicate that including a pitch-angle dependence in the simulations reduces the agreement with observations for the simulation window presented here. However, the influence of the a pitch-angle dependence is less pronounced in 3-D simulations.

4.4. Simulations of Different Period

In addition to the results described above, we simulate a different period, ranging from January 1, 2015 until January 1, 2016. The geomagnetic activity during 2015 is higher than during the 2012–2013 simulation window, with a median Kp-index of 2, reaching a maximum value of 8.3, compared to a median Kp of 1.3, reaching a maximum value of 7. Figure 10 is similar to Figure 3, and shows the results of 3-D simulations at an energy of 1.01 MeV. In general, we reach similar conclusions when comparing the simulations and observations, as discussed in Section 3.2. Simulations with different radial diffusion coefficients provide similar agreement with observations of the 1.01 MeV electron flux, with an exception of simulation with D_{LL}^{A}. The average across all energies $|ND|$ with corresponding diffusion coefficients are 33% (D_{LL}^{BA}), 33% (D_{LL}^{O}), 46% (D_{LL}^{A}), 35% (D_{LL}^{L}), and 37% ($D_{LL}^{BE(CRESS)}+D_{LL}^{AM(CRESS)}$). Figures S9 and S10 complement Figure 10, displaying results of 3-D simulations at energies of 596 keV and 4.2 MeV.

Similar to Figure 4, we show the comparison of the average normalized difference across multiple energies in Figure 11. The simulations with D_{LL}^{A} resulted in the largest error in both 1-D and 3-D simulations. The difference between 1-D simulations appears to be larger that in 3-D. The simulation flux modeled in 1-D, of ~ 1 MeV electrons (Figure S7) is lower than the observations for much of the outer radiation belt, which illustrates the effect of the absence of local acceleration. The lowest average normalized difference is observed in the simulations with D_{LL}^{BA}. For the interested reader, Figures S6 and S8 show the electron flux obtained from 1-D simulations at energies 596 keV, and 4.2 MeV, in comparison to measurements.

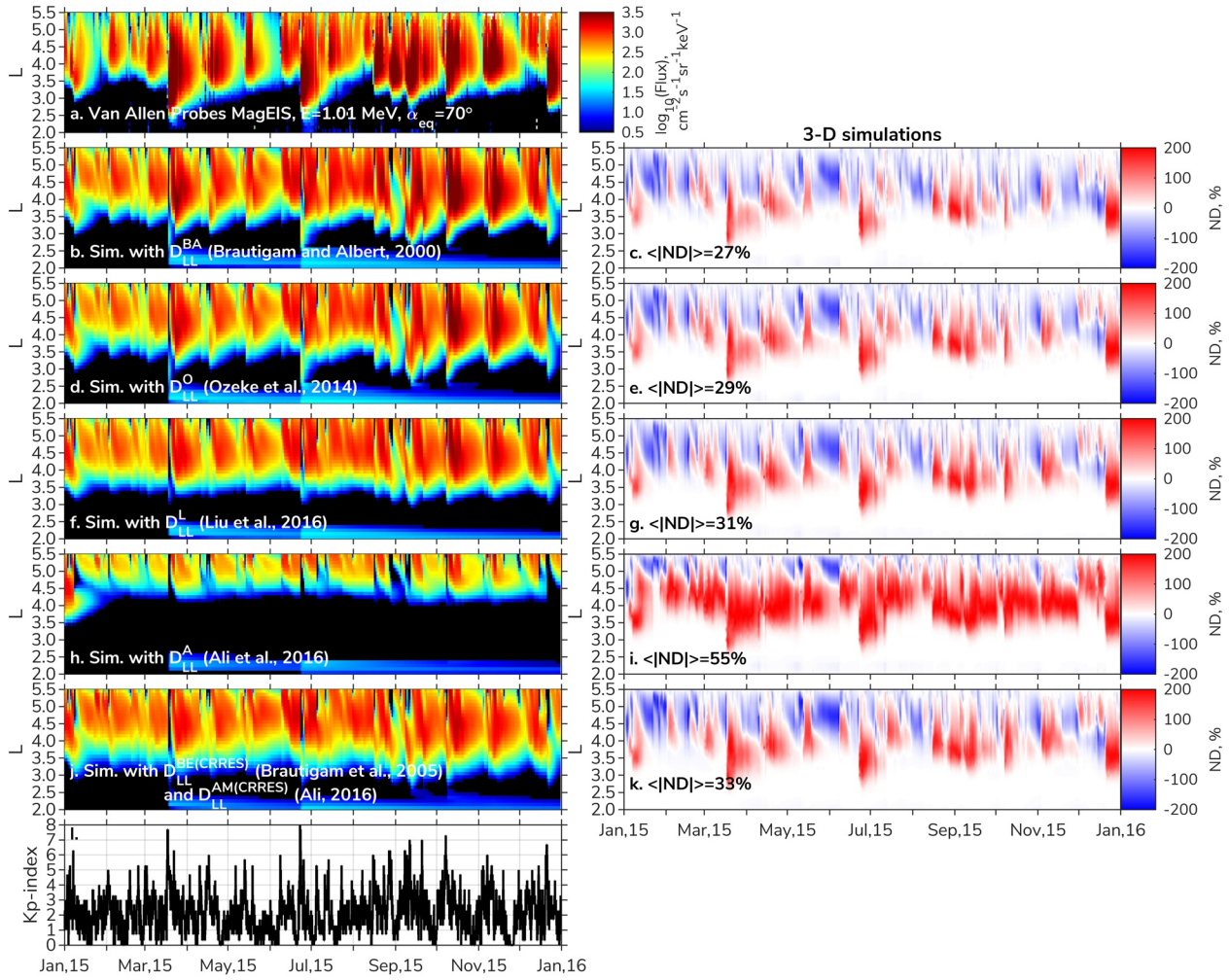

Figure 10. Same as Figure 3, but 3-D simulations are performed for the period from January 1, 2015 until January 1, 2016, and measurements (panel a) of electron flux at 1.01 MeV, from Magnetic Electron Ion Spectrometer (MagIES) instrument, are presented for the same period.

5. Conclusions

In this study, we have tested D_{LL} parameterizations (Ali, 2016; Ali et al., 2016; Brautigam & Albert, 2000; Brautigam et al., 2005; Liu et al., 2016; Ozeke et al., 2014), in 1-D and 3-D radiation belt long-term modeling, considering different periods of the 24th solar cycle. The simulation results have been compared, both to one another, and to observations. Our key findings are as follows:

1. The difference between 3-D simulations with $D_{LL}^{BA}, D_{LL}^{O}, D_{LL}^{L}, D_{LL}^{BE(CRRES)} + D_{LL}^{AM(CRRES)}$ parameterizations is small. We suggest that the output from radiation belt models using any of these parameterizations will likely show a similar L^* structure to observations.
2. 3-D simulations are observed to be less sensitive to the assumed parameterization of the radial diffusion rates than 1-D simulations.
3. Simulations using D_{LL}^{A} showed 1 MeV flux levels significantly lower than observations with an outer radiation belt that did not extend below $L^* < 4$.
4. The simulation with μ-dependent D_{LL}^{L}, not limited to $\mu \geq 400$ MeV/G, resulted in larger flux peaks and produced a remnant belt between $2 < L^* < 2.5$ that is absent in the measurements. Ignoring the μ dependence of the Liu et al. (2016) coefficients (assuming the value corresponding to $\mu = 1000\ MeV\ /\ G$ for all μ) yielded less inward diffusion overall and reduced the agreement with MagEIS flux values. The best agreement is achieved by holding D_{LL}^{L} constant with $\mu = 400$ MeV/G for the lower values of μ.

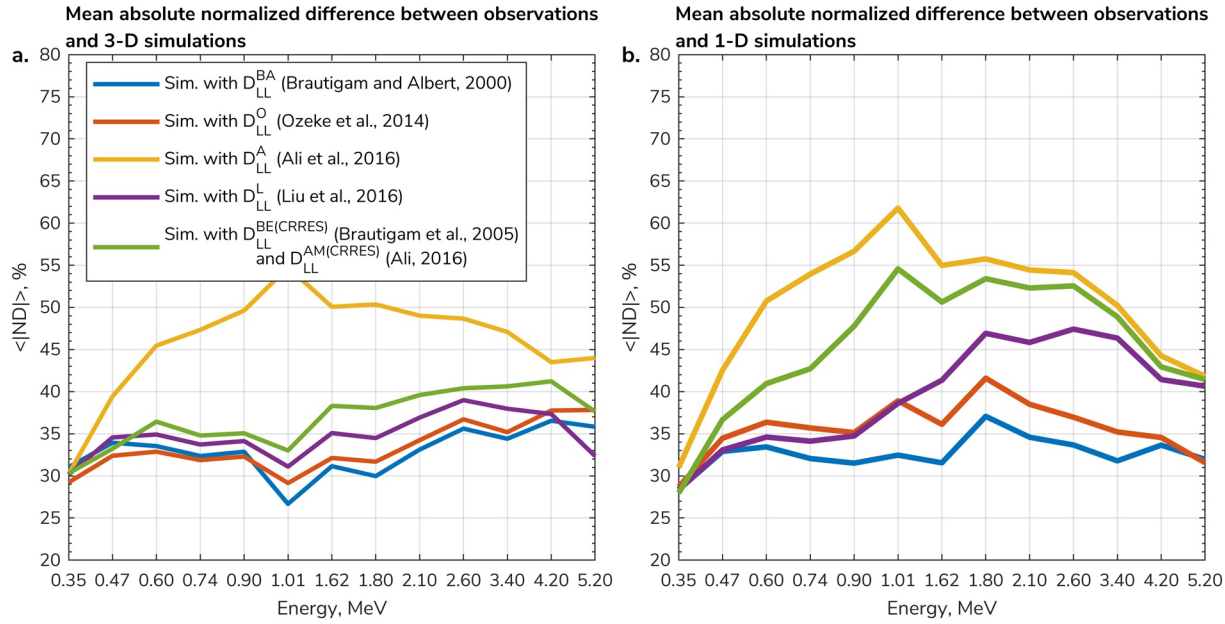

Figure 11. Same as Figure 4, but 1-D and 3-D simulations are performed for the period from January 1, 2015 until January 1, 2016. The dashed lines (simulations without electromagnetic ion cyclotron (EMIC) waves) are not presented.

5. The mean absolute value of the normalized difference averaged across energies suggests that 3-D simulations using the Brautigam and Albert (2000) coefficient provide the smallest overall difference between simulation results and observations ($\left|ND\right|$ = 32%–33%). However, this value was comparable to that achieved in the model runs using the Ozeke et al. (2014) ($\left|ND\right|$ =33%) and Liu et al. (2016) ($\left|ND\right|$ =33%–35% parameterizations. The simulation using a parameterization derived from the CRRES era (Ali, 2016; Brautigam et al., 2005) also gave comparable but marginally larger values ($\left|ND\right|$ = 36%–37%).
6. We present an open question as to whether the pitch angle scaling of (Schulz, 1991) can be applied to D_{LL} coefficients derived using the Fei et al. (2006) formalism. Our results suggest that, for the Brautigam and Albert (2000) coefficient, the pitch angle scaling reduces the agreement with observations in the 1-D simulation and does not substantially influence the result of the 3-D simulation.
7. For the simulation of the 2015 period, the 1-D simulations showed more dependence on the D_{LL} parameterization selected than was seen for the October 2012 to October 2013 period. We attribute this to the higher geomagnetic activity in 2015. The 3-D simulations during both periods were less sensitive to the selection of D_{LL}.

A clear understanding of how various radial diffusion coefficients perform is vital, both from a modeling standpoint, but additionally for understanding the impact of using different formalisms, such as an electromagnetic diffusion coefficient, separate electric and magnetic components, or neglecting the magnetic component altogether (e.g., Brautigam & Albert, 2000; Fei et al., 2006). We suggest that, as new parameterizations for radial diffusion coefficients are developed, they should also be bench-marked against pre-existing values to monitor progression in performance.

Data Availability Statement

The authors used geomagnetic indices provided by OMNIWeb (https://omniweb.gsfc.nasa.gov/) and are grateful to the RBSP-ECT team for the provision of Van Allen Probes observations (https://rbsp-ect.lanl.gov/). The data to reproduce the figures are available at UCLA dataverse repository (https://doi.org/10.25346/S6/U9WFPD).

Acknowledgments
This research is supported by NASA awards 80NSSC18K0663. H.J. Allison acknowledges support from the Alexander von Humboldt Association. This project has received funding from the European Union's Horizon 2020 research and innovation programme under grant agreement No. 870452 (PAGER). The authors would like to thank Michael Schulz, Dmitry Subbotin, Ksenia Orlova, Hui Zhu, Dedong Wang, Anthony Saikin, Artem Smirnov, Adam Kellerman, Geoff Reeves and Larry Lyons for useful discussions. This work used computational and storage services associated with the Hoffman2 Shared Cluster provided by UCLA Institute for Digital Research and Education's Research Technology Group. The authors also acknowledge the developers of the International Radiation Belt Environment Modeling (IRBEM) library. The authors would like to thank Sharon Uy for proofreading this manuscript.
Open access funding enabled and organized by Projekt DEAL.

References

Ali, A. F. (2016). *ULF waves and diffusive radial transport of charged particles (Unpublished doctoral dissertation)*. Faculty of the Graduate School of the University of Colorado.

Ali, A. F., Elkington, S. R., Tu, W., Ozeke, L. G., Chan, A. A., & Friedel, R. H. W. (2015). Magnetic field power spectra and magnetic radial diffusion coefficients using CRRES magnetometer data. *Journal of Geophysical Research: Space Physics*, *120*, 973–995. https://doi.org/10.1002/2014JA020419

Ali, A. F., Malaspina, D. M., Elkington, S. R., Jaynes, A. N., Chan, A. A., Wygant, J., & Kletzing, C. A. (2016). Electric and magnetic radial diffusion coefficients using the Van Allen probes data. *Journal of Geophysical Research: Space Physics*, *121*, 9586–9607. https://doi.org/10.1002/2016JA023002

Allison, H. J., Shprits, Y. Y., Zhelavskaya, I. S., Wang, D., & Smirnov, A. G. (2021). Gyroresonant wave-particle interactions with chorus waves during extreme depletions of plasma density in the Van Allen radiation belts. *Science Advances*, *7*(5). https://doi.org/10.1126/sciadv.abc0380

Baker, D. N., Kanekal, S. G., Hoxie, V. C., Batiste, S., Bolton, M., Li, X., et al. (2013). The relativistic Electron-Proton telescope (REPT) instrument on board the radiation belt storm probes (RBSP) spacecraft: Characterization of Earth's radiation belt High-Energy particle populations. *Space Science Reviews*, *179*(1–4), 337–381. https://doi.org/10.1007/s11214-012-9950-9

Barani, M., Tu, W., Sarris, T., Pham, K., & Redmon, R. J. (2019). Estimating the azimuthal mode structure of ULF waves based on multiple GOES satellite observations. *Journal of Geophysical Research: Space Physics*, *124*, 5009–5026. https://doi.org/10.1029/2019JA026927

Bentley, S. N., Watt, C. E. J., Owens, M. J., & Rae, I. J. (2018). Ulf wave activity in the magnetosphere: Resolving solar wind interdependencies to identify driving mechanisms. *Journal of Geophysical Research: Space Physics*, *123*, 2745–2771. https://doi.org/10.1002/2017ja024740

Blake, J. B., Carranza, P. A., Claudepierre, S. G., Clemmons, J. H., Crain, W. R., Jr, Dotan, Y., et al. (2013). The magnetic electron ion spectrometer (MagEIS) instruments aboard the radiation belt storm probes (RBSP) spacecraft. *Space Science Reviews*, *179*(1–4), 383–421. https://doi.org/10.1007/s11214-013-9991-8

Brautigam, D. H., & Albert, J. M. (2000). Radial diffusion analysis of outer radiation belt electrons during the october 9, 1990, magnetic storm. *Journal of Geophysical Research*, *105*(A1), 291–309. https://doi.org/10.1029/1999ja900344

Brautigam, D. H., Ginet, G. P., Albert, J. M., Wygant, J. R., Rowland, D. E., Ling, A., & Bass, J. (2005). CRRES electric field power spectra and radial diffusion coefficients. *Journal of Geophysical Research*, *110*(A2), A02214. https://doi.org/10.1029/2004JA010612

Brizard, A. J., & Chan, A. A. (2001). Relativistic bounce-averaged quasilinear diffusion equation for low-frequency electromagnetic fluctuations. *Physics of Plasmas*, *8*(11), 4762–4771. https://doi.org/10.1063/1.1408623

Califf, S., & Cully, C. M. (2016). Empirical estimates and theoretical predictions of the shorting factor for the THEMIS double-probe electric field instrument: THEMIS shorting factor. *Journal of Geophysical Research: Space Physics*, *121*, 6223–6233. https://doi.org/10.1002/2016JA022589

Califf, S., Li, X., Blum, L., Jaynes, A., Schiller, Q., Zhao, H., et al. (2014). THEMIS measurements of quasi-static electric fields in the inner magnetosphere. *Journal of Geophysical Research: Space Physics*, *119*, 9939–9951. https://doi.org/10.1002/2014JA020360

Carpenter, D. L., & Anderson, R. R. (1992). An ISEE/whistler model of equatorial electron density in the magnetosphere. *Journal of Geophysical Research*, *97*(A2), 1097–1108. https://doi.org/10.1029/91JA01548

Cornwall, J. M. (1968). Diffusion processes influenced by conjugate-point wave phenomena. *Radio Science*, *3*(7), 740–744. https://doi.org/10.1002/rds196837740

Drozdov, A. Y., Shprits, Y. Y., Aseev, N. A., Kellerman, A. C., & Reeves, G. D. (2017). Dependence of radiation belt simulations to assumed radial diffusion rates tested for two empirical models of radial transport. *Space Weather*, *15*(1), 150–162. https://doi.org/10.1002/2016SW001426

Drozdov, A. Y., Shprits, Y. Y., Usanova, M. E., Aseev, N. A., Kellerman, A. C., & Zhu, H. (2017). EMIC wave parameterization in the long-term VERB code simulation. *Journal of Geophysical Research: Space Physics*, *122*, 8488–8501. https://doi.org/10.1002/2017JA024389

Drozdov, A. Y., Usanova, M. E., Hudson, M. K., Allison, H. J., & Shprits, Y. Y. (2020). The role of hiss, chorus, and EMIC waves in the modeling of the dynamics of the Multi-MeV radiation belt electrons. *Journal of Geophysical Research: Space Physics*, *125*, e2020JA028282. https://doi.org/10.1029/2020JA028282

Elkington, S. R., Chan, A. A., & Wiltberger, M. (2012). Global structure of ULF waves during the 24-26 September 1998 geomagnetic storm: Summers/Dynamics of the Earth's radiation belts and inner magnetosphere. In D. Summers, I. R. Mann, D. N. Baker, & M. Schulz (Eds.), *Dynamics of the earth's radiation belts and inner magnetosphere* (pp. 127–138). Washington, DC. American Geophysical Union. https://doi.org/10.1029/2012GM001348

Elkington, S. R., Hudson, M. K., & Chan, A. A. (1999). Acceleration of relativistic electrons via drift-resonant interaction with toroidal-mode pc-5 ULF oscillations. *Geophysical Research Letters*, *26*(21), 3273–3276. https://doi.org/10.1029/1999gl003659

Elkington, S. R., Hudson, M. K., & Chan, A. A. (2003). Resonant acceleration and diffusion of outer zone electrons in an asymmetric geomagnetic field. *Journal of Geophysical Research*, *108*(A3), 1116. https://doi.org/10.1029/2001JA009202

Fälthammar, C. G. (1965). Effects of time-dependent electric fields on geomagnetically trapped radiation. *Journal of Geophysical Research*, *70*(11), 2503–2516. https://doi.org/10.1029/jz070i011p02503

Fälthammar, C. G. (1968). Radial diffusion by violation of the third adiabatic invariant, earth's particles and fields. In B. M. McCormac (Ed.), *Earth's particles and fields* (pp. 157–169). New York. Reinhold.

Fei, Y., Chan, A. A., Elkington, S. R., & Wiltberger, M. J. (2006). Radial diffusion and mhd particle simulations of relativistic electron transport by ULF waves in the September 1998 storm. *Journal of Geophysical Research*, *111*(A12), A12209. https://doi.org/10.1029/2005ja011211

Glauert, S. A., Horne, R. B., & Meredith, N. P. (2014). Simulating the Earth's radiation belts: Internal acceleration and continuous losses to the magnetopause. *Journal of Geophysical Research: Space Physics*, *119*, 7444–7463. https://doi.org/10.1002/2014JA020092

Gu, X., Shprits, Y. Y., & Ni, B. (2012). Parameterized lifetime of radiation belt electrons interacting with lower-band and upper-band oblique chorus waves. *Geophysical Research Letters*, *39*(15), L15102. https://doi.org/10.1029/2012GL052519

Holzworth, R. H., & Mozer, F. S. (1979). Direct evaluation of the radial diffusion coefficient near l = 6 due to electric field fluctuations. *Journal of Geophysical Research*, *84*(A6), 2559. https://doi.org/10.1029/JA084iA06p02559

Horne, R. B., Thorne, R. M., Glauert, S. A., Albert, J. M., Meredith, N. P., & Anderson, R. R. (2005). Timescale for radiation belt electron acceleration by whistler mode chorus waves. *Journal of Geophysical Research*, *110*, A03225. https://doi.org/10.1029/2004ja010811

Jacobs, J. A., Kato, Y., Matsushita, S., & Troitskaya, V. A. (1964). Classification of geomagnetic micropulsations. *Journal of Geophysical Research*. 1896-1977, *69*(1), 180–181. https://doi.org/10.1029/JZ069i001p00180

Jaynes, A. N., Ali, A. F., Elkington, S. R., Malaspina, D. M., Baker, D. N., Li, X., et al. (2018). Fast diffusion of ultrarelativistic electrons in the outer radiation belt: 17 march 2015 storm event. *Geophysical Research Letters*, *45*, 10874–10882. https://doi.org/10.1029/2018GL079786

Kim, H.-J., Lee, D.-Y., Wolf, R., Bortnik, J., Kim, K.-C., Lyons, L., et al. (2021). Rapid injections of mev electrons and extremely fast step-like outer radiation belt enhancements. *Geophysical Research Letters*, *48*, e2021GL093151. https://doi.org/10.1029/2021GL093151

Kim, K.-C., Shprits, Y., Subbotin, D., & Ni, B. (2011). Understanding the dynamic evolution of the relativistic electron slot region including radial and pitch angle diffusion. *Journal of Geophysical Research*, *116*, A10214. https://doi.org/10.1029/2011JA016684

Lanzerotti, L. J., & Morgan, C. G. (1973). ULF geomagnetic power near l = 4: 2. temporal variation of the radial diffusion coefficient for relativistic electrons. *Journal of Geophysical Research*, *78*, 4600–4610. https://doi.org/10.1029/ja078i022p04600

Lejosne, S., Boscher, D., Maget, V., & Rolland, G. (2013). Deriving electromagnetic radial diffusion coefficients of radiation belt equatorial particles for different levels of magnetic activity based on magnetic field measurements at geostationary orbit. *Journal of Geophysical Research: Space Physics*, *118*, 3147–3156. https://doi.org/10.1002/jgra.50361

Lejosne, S., & Kollmann, P. (2019). Radiation belt radial diffusion at earth and beyond. *Earth and Space Science Open Archive*. https://doi.org/10.1002/essoar.10501074.1

Li, W., Ma, Q., Thorne, R. M., Bortnik, J., Zhang, X.-J., Li, J., et al. (2016). Radiation belt electron acceleration during the 17 March 2015 geomagnetic storm: Observations and simulations. *Journal of Geophysical Research: Space Physics*, *121*, 5520–5536. https://doi.org/10.1002/2016JA022400

Li, Z., Hudson, M., Paral, J., Wiltberger, M., & Turner, D. (2016). Global ULF wave analysis of radial diffusion coefficients using a global MHD model for the 17 March 2015 storm: Radial diffusion coefficient calculation. *Journal of Geophysical Research: Space Physics*, *121*, 6196–6206. https://doi.org/10.1002/2016JA022508

Li, Z., Hudson, M., Patel, M., Wiltberger, M., Boyd, A., & Turner, D. (2017). ULF wave analysis and radial diffusion calculation using a global MHD model for the 17 March 2013 and 2015 storms. *Journal of Geophysical Research: Space Physics*, *122*, 7353–7363. https://doi.org/10.1002/2016JA023846

Liu, W., Tu, W., Li, X., Sarris, T., Khotyaintsev, Y., Fu, H., et al. (2016). On the calculation of electric diffusion coefficient of radiation belt electrons with in situ electric field measurements by THEMIS. *Geophysical Research Letters*, *43*(3), 1023–1030. https://doi.org/10.1002/2015GL067398

Mager, P. N., & Klimushkin, D. Y. (2005). Spatial localization and azimuthal wave numbers of alfvén waves generated by drift-bounce resonance in the magnetosphere. *Annales Geophysicae*, *23*(12), 3775–3784. https://doi.org/10.5194/angeo-23-3775-2005

Malaspina, D. M., Claudepierre, S. G., Takahashi, K., Jaynes, A. N., Elkington, S. R., Ergun, R. E., et al. (2015). Kinetic Alfvén waves and particle response associated with a shock-induced, global ULF perturbation of the terrestrial magnetosphere: Kaw from shock impact. *Geophysical Research Letters*, *42*, 9203–9212. https://doi.org/10.1002/2015GL065935

McIlwain, C. E. (1961). Coordinates for mapping the distribution of magnetically trapped particles. *Journal of Geophysical Research*, *66*(11), 3681–3691. https://doi.org/10.1029/JZ066i011p03681

Miyoshi, Y. S., Jordanova, V. K., Morioka, A., Thomsen, M. F., Reeves, G. D., Evans, D. S., & Green, J. C. (2006). Observations and modeling of energetic electron dynamics during the october 2001 storm. *Journal of Geophysical Research*, *111*(A11), A11S02. https://doi.org/10.1029/2005JA011351

Murphy, K. R., Mann, I. R., Rae, I. J., Sibeck, D. G., & Watt, C. E. J. (2016). Accurately characterizing the importance of wave-particle interactions in radiation belt dynamics: The pitfalls of statistical wave representations. *Journal of Geophysical Research: Space Physics*, *121*, 7895–7899. https://doi.org/10.1002/2016JA022618

Ni, B., Thorne, R. M., Shprits, Y. Y., & Bortnik, J. (2008). Resonant scattering of plasma sheet electrons by whistler-mode chorus: Contribution to diffuse auroral precipitation. *Geophysical Research Letters*, *35*, L11106. https://doi.org/10.1029/2008gl034032

Olifer, L., Mann, I. R., Ozeke, L. G., Rae, I. J., & Morley, S. K. (2019). On the relative strength of electric and magnetic ULF wave radial diffusion during the March 2015 geomagnetic storm. *Journal of Geophysical Research: Space Physics*, *124*, 2569–2587. https://doi.org/10.1029/2018JA026348

Orlova, K., Shprits, Y., & Spasojevic, M. (2016). New global loss model of energetic and relativistic electrons based on Van Allen probes measurements. *Journal of Geophysical Research: Space Physics*, *121*, 1308–1314. https://doi.org/10.1002/2015JA021878

Orlova, K., & Shprits, Y. Y. (2011). On the bounce-averaging of scattering rates and the calculation of bounce period. *Physics of Plasmas*, *18*(9), 092904. https://doi.org/10.1063/1.3638137

Orlova, K., Shprits, Y. Y., & Ni, B. (2012). Bounce-averaged diffusion coefficients due to resonant interaction of the outer radiation belt electrons with oblique chorus waves computed in a realistic magnetic field model. *Journal of Geophysical Research: Space Physics*, *117*, A07209. https://doi.org/10.1029/2012JA017591

Orlova, K., Spasojevic, M., & Shprits, Y. (2014). Activity-dependent global model of electron loss inside the plasmasphere. *Geophysical Research Letters*, *41*(11), 3744–3751. https://doi.org/10.1002/2014GL060100

Ozeke, L. G., & Mann, I. R. (2001). Modeling the properties of high- m alfvén waves driven by the drift-bounce resonance mechanism. *Journal of Geophysical Research*, *106*(A8), 15583–15597. https://doi.org/10.1029/2000JA000393

Ozeke, L. G., Mann, I. R., Murphy, K. R., Jonathan Rae, I., & Milling, D. K. (2014). Analytic expressions for ULF wave radiation belt radial diffusion coefficients. *Journal of Geophysical Research: Space Physics*, *119*, 1587–1605. https://doi.org/10.1002/2013JA019204

Ozeke, L. G., Mann, I. R., Murphy, K. R., Rae, I. J., Milling, D. K., Elkington, S. R., et al. (2012). ULF wave derived radiation belt radial diffusion coefficients. *Journal of Geophysical Research: Space Physics*, *117*, A04222. https://doi.org/10.1029/2011JA017463

Ozeke, L. G., Mann, I. R., Olifer, L., Dufresne, K. Y., Morley, S. K., Claudepierre, S. G., et al. (2020). Rapid outer radiation belt flux dropouts and fast acceleration during the March 2015 and 2013 storms: The role of ultra-low frequency wave transport from a dynamic outer boundary. *Journal of Geophysical Research: Space Physics*, *125*, e2019JA027179. https://doi.org/10.1029/2019JA027179

Perry, K. L., Hudson, M. K., & Elkington, S. R. (2005). Incorporating spectral characteristics of Pc5 waves into three-dimensional radiation belt modeling and the diffusion of relativistic electrons. *Journal of Geophysical Research*, *110*(A3), 14853. https://doi.org/10.1029/2004JA010760

Ripoll, J.-F., Reeves, G. D., Cunningham, G. S., Loridan, V., Denton, M., Santolík, O., et al. (2016). Reproducing the observed energy-dependent structure of earth's electron radiation belts during storm recovery with an event-specific diffusion model: Energy-Dependent structure of the belts. *Geophysical Research Letters*, *43*, 5616–5625. https://doi.org/10.1002/2016gl068869

Roederer, J. G. (1970). *Dynamics of geomagnetically trapped radiation*. Springer Berlin Heidelberg. https://doi.org/10.1007/978-3-642-49300-3

Sarris, T. E., Li, X., Liu, W., Argyriadis, E., Boudouridis, A., & Ergun, R. (2013). Mode number calculations of ULF field-line resonances using ground magnetometers and THEMIS measurements: Mode number of ULF field-line resonances. *Journal of Geophysical Research: Space Physics*, *118*, 6986–6997. https://doi.org/10.1002/2012JA018307

Schulz, M. (1991). 2 - The magnetosphere. In J. A. Jacobs (Ed.), *Geomagnetism* (pp. 87–293). London. Academic Press. https://doi.org/10.1016/B978-0-12-378674-6.50008-X

Schulz, M., & Eviatar, A. (1969). Diffusion of equatorial particles in the outer radiation zone. *Journal of Geophysical Research*, *74*(9), 2182–2192. https://doi.org/10.1029/JA074i009p02182

Schulz, M., & Lanzerotti, L. J. (1974). *Particle diffusion in the radiation belts* (Vol. 7). Springer.

Shprits, Y. Y., Elkington, S. R., Meredith, N. P., & Subbotin, D. A. (2008). Review of modeling of losses and sources of relativistic electrons in the outer radiation belt I: Radial transport. *Journal of Atmospheric and Solar-Terrestrial Physics*, *70*(14), 1679–1693. https://doi.org/10.1016/j.jastp.2008.06.008

Shprits, Y. Y., Kellerman, A. C., Drozdov, A. Y., Spence, H. E., Reeves, G. D., & Baker, D. N. (2015). Combined convective and diffusive simulations: VERB-4D comparison with 17 March 2013 Van Allen Probes observations. *Geophysical Research Letters*, *42*, 9600–9608. https://doi.org/10.1002/2015GL065230

Shprits, Y. Y., & Ni, B. (2009). Dependence of the quasi-linear scattering rates on the wave normal distribution of chorus waves. *Journal of Geophysical Research*, *114*, A11205. https://doi.org/10.1029/2009ja014223

Shprits, Y. Y., Thorne, R. M., Friedel, R., Reeves, G. D., Fennell, J., Baker, D. N., & Kanekal, S. G. (2006). Outward radial diffusion driven by losses at magnetopause. *Journal of Geophysical Research*, *111*, A11214. https://doi.org/10.1029/2006JA011657

Stratton, J. M., Harvey, R. J., & Heyler, G. A. (2013). Mission overview for the radiation belt storm probes mission. *Space Science Reviews*, *179*(1), 29–57. https://doi.org/10.1007/s11214-012-9933-x

Subbotin, D. A., & Shprits, Y. Y. (2009). Three-dimensional modeling of the radiation belts using the versatile electron radiation belt (VERB) code. *Space Weather*, *7*(10). https://doi.org/10.1029/2008SW000452

Subbotin, D. A., & Shprits, Y. Y. (2012). Three-dimensional radiation belt simulations in terms of adiabatic invariants using a single numerical grid. *Journal of Geophysical Research*, *117*, A05205. https://doi.org/10.1029/2011JA017467

Subbotin, D. A., Shprits, Y. Y., & Ni, B. (2011). Long-term radiation belt simulation with the VERB 3-D code: Comparison with CRRES observations. *Journal of Geophysical Research*, *116*, A12210. https://doi.org/10.1029/2011JA017019

Takahashi, K., & Anderson, B. J. (1992). Distribution of ULF energy (f<80 mhz) in the inner magnetosphere: A statistical analysis of AMPTE CCE magnetic field data. *Journal of Geophysical Research*, *97*(A7), 10751. https://doi.org/10.1029/92JA00328

Thorne, R. M., Li, W., Ni, B., Ma, Q., Bortnik, J., Chen, L., et al. (2013). Rapid local acceleration of relativistic radiation-belt electrons by magnetospheric chorus. *Nature*, *504*, 411–414. https://doi.org/10.1038/nature12889

Tsyganenko, N. A., & Sitnov, M. I. (2005). Modeling the dynamics of the inner magnetosphere during strong geomagnetic storms. *Journal of Geophysical Research*, *110*, 7737. https://doi.org/10.1029/2004JA010798

Tsyganenko, N. A., & Sitnov, M. I. (2007). Magnetospheric configurations from a high-resolution data-based magnetic field model. *Journal of Geophysical Research*, *112*, A06225. https://doi.org/10.1029/2007JA012260

Tu, W., Elkington, S. R., Li, X., Liu, W., & Bonnell, J. (2012). Quantifying radial diffusion coefficients of radiation belt electrons based on global MHD simulation and spacecraft measurements: Quantify radial diffusion coefficients. *Journal of Geophysical Research*, *117*, e2019JA027634. https://doi.org/10.1029/2012JA017901

Tu, W., Xiang, Z., & Morley, S. K. (2019). Modeling the magnetopause shadowing loss during the June 2015 dropout event. *Geophysical Research Letters*, *46*(16), 9388–9396. https://doi.org/10.1029/2019gl084419

Ukhorskiy, A. Y., & Sitnov, M. I. (2013). Dynamics of radiation belt particles. *Space Science Reviews*, *179*(1), 545–578. https://doi.org/10.1007/s11214-012-9938-5

Ukhorskiy, A. Y., Sitnov, M. I., Takahashi, K., & Anderson, B. J. (2009). Radial transport of radiation belt electrons due to stormtime Pc5 waves. *Annales Geophysicae*, *27*(5), 2173–2181. https://doi.org/10.5194/angeo-27-2173-2009

Ukhorskiy, A. Y., Takahashi, K., Anderson, B. J., & Korth, H. (2005). Impact of toroidal ULF waves on the outer radiation belt electrons. *Journal of Geophysical Research*, *110*(A10), 128. https://doi.org/10.1029/2005JA011017

Wang, D., Shprits, Y. Y., Zhelavskaya, I. S., Effenberger, F., Castillo, A., Drozdov, A. Y., et al. (2020). The effect of plasma boundaries on the dynamic evolution of relativistic radiation belt electrons. *Journal of Geophysical Research: Space Physics*, *125*, e2019JA027422. https://doi.org/10.1029/2019JA027422

Watt, C. E. J., Rae, I. J., Murphy, K. R., Anekallu, C., Bentley, S. N., & Forsyth, C. (2017). The parameterization of wave-particle interactions in the outer radiation belt. *Journal of Geophysical Research: Space Physics*, *122*(9), 9545–9551. https://doi.org/10.1002/2017ja024339